The Normal Examination

1

Contents

1.1 Introduction

Echocardiography together with the different modalities of Doppler examination has become the most important noninvasive method for assessment of the heart in children (Daubeney et al. 1999; DeGroff et al. 2002; Higgins et al. 1990; Lai et al. 2006; Lai and Mertens et al. 2009; Mertens et al. 2010; Skinner et al. 2000; Snider et al. 1997). It is dependent on the presence of acoustic windows, allowing access of the ultrasound beam to the heart without the interference of air or skeletal structures. In the paediatric age group, echocardiography is greatly enhanced by the fact that the physical conditions and the acoustic windows for examination of the heart are much more favourable than in adults: shorter distances between the body surface and the heart and great vessels allow the application of high frequency transducers with excellent resolution in neonates and infants. In addition the subcostal window provides excellent conditions to visualize the heart in infants and children (Fig. 1.1). The precordial window is significantly larger in children due to less hyperinflation of the lungs and incomplete calcification of the sternum in young infants. Furthermore the large thymus gland in neonates and infants enlarges the acoustic window to the great vessels from the suprasternal and high parasternal views.

The following chapter provides an introduction into the different planes for two-dimensional and Doppler echocardiography and into the basics of colour Doppler and pulsed wave and continuous wave Doppler examination of the heart.

1.2 2D Echo and Colour Doppler Echocardiography

1.2.1 Parasternal Views

These views are obtained by placement of the transducer in the third left intercostal space close to the sternum (Fig. 1.2). For the *parasternal long-axis views*, the plane is oriented

Electronic supplementary material The online version of this chapter (doi:10.1007/978-3-319-42919-9_1) contains supplementary material, which is available to authorized users.

M. Hofbeck et al., *Doppler Echocardiography in Infancy and Childhood*, DOI 10.1007/978-3-319-42919-9_1

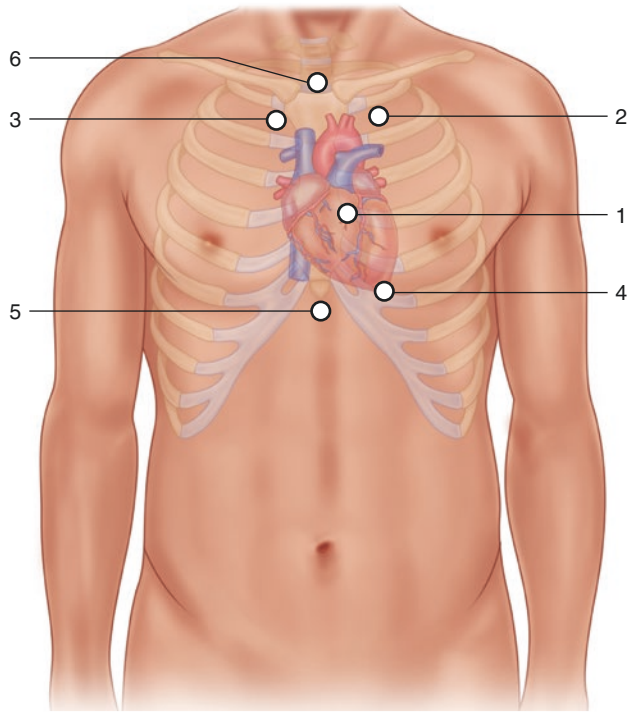

Fig. 1.1 Diagram depicting echocardiographic windows in children including the parasternal *1*, high left parasternal *2* and high right parasternal *3*, the apical *4*, subcostal *5* and suprasternal *6* windows

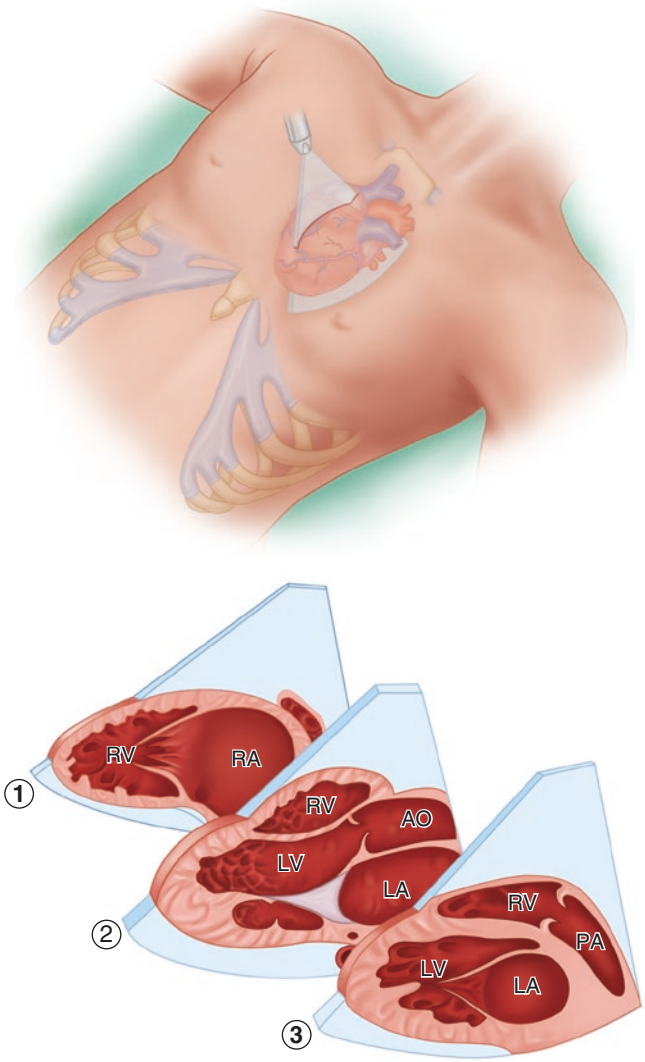

Fig. 1.2 Parasternal long-axis views with planes of the right ventricular inflow *1*, left ventricle *2* and right ventricular outflow tract *3*. *RV* right ventricle, *RA* right atrium, *LV* left ventricle

along the major axis of the heart with an external orientation from the patient's left hip to the right shoulder (Lai et al. 2006; Lai and Ko 2009; Snider et al. 1997).

The standard parasternal long axis displays a longitudinal section of the left ventricle and its outflow tract. The aortic valve and the mitral valve are depicted in the centre of the image displaying fibrous continuity between the anterior leaflet of the mitral valve and the posterior wall of the aortic root (Fig 1.3, Video 1.1). This plane is useful for the colour Doppler interrogation both of the aortic and of the mitral valves (Fig. 1.3b, c). While the angle of insonation is not really favourable for pulsed wave or continuous wave Doppler interrogation, the high velocities encountered in stenosis or leakage of aortic or mitral valve allow detection of regurgitant or turbulent flow in this plane. In the presence of aortic stenosis, accelerated flow and turbulence will be noted in the ascending aorta, and in the presence of aortic insufficiency, the regurgitant jet will be depicted in the left ventricle.

Tilting of the transducer towards the patient's right hip brings into view the parasternal long axis of the right ventricular inflow (Lai et al. 2006; Lai and Ko 2009; Snider et al. 1997) (Video 1.2). This plane shows the tricuspid valve with its inferior and anterior leaflet as well as the coronary sinus draining into the right atrium (Fig. 1.4, Video 1.3). Colour Doppler examination in this plane allows interrogation of the right ventricular inflow and verification of tricuspid regurgitation. In the presence of tricuspid regurgitation, PW and CW Doppler can be employed for quantification of the velocity of the regurgitant jet.

Back to the standard parasternal long axis of the left ventricle, tilting of the transducer in the opposite direction towards the patient's left shoulder opens the right ventricular outflow tract and the main pulmonary artery (Fig. 1.5, Video

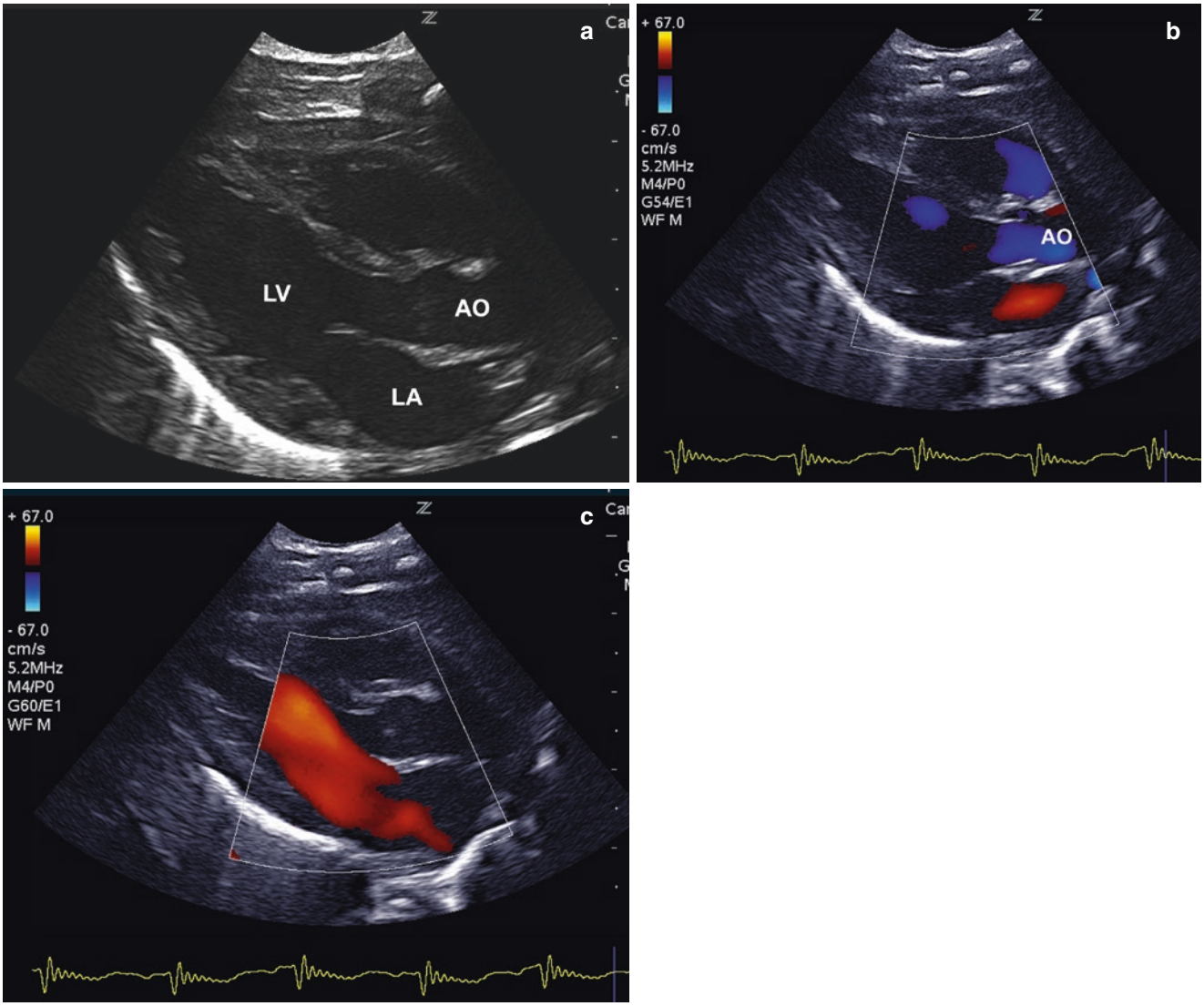

Fig. 1.3 Parasternal long-axis view of the left ventricle (*LV*) showing the inflow and the outflow tract (**a**). The left atrium (*LA*) is displayed behind the aorta (*AO*). Colour Doppler examination shows forward flow in the aorta during systole (**b**) and forward flow across the mitral valve during diastole (**c**)

1.4). Due to the favourable angle of insonation, this plane is well suited for colour Doppler and continuous and pulsed wave Doppler interrogation of the right ventricular outflow tract, the pulmonary valve and the main pulmonary artery (Videos 1.5 and 1.6).

The *parasternal short-axis views* are obtained by 90° clockwise rotation of the transducer from the parasternal long-axis view of the left ventricle (Fig. 1.6). This results in a scanning plane oriented from the patient's right hip to the left shoulder (Snider et al. 1997). Tilting of the transducer offers a family of different short-axis planes from the base of the heart to the apex (Lai et al. 2006; Lai and Ko 2009; Snider et al. 1997). The parasternal short-axis view of the base of the heart depicts the aortic valve in the centre of the image (Video 1.7). This plane allows visualization of the aortic valve cusps and their respective sinuses as well as the origin of the coronary arteries (Fig 1.7). The left atrium is displayed behind the aorta. Furthermore it shows the connection of the right atrium to the right ventricle, the right ventricular outflow tract, the pulmonary valve and the main

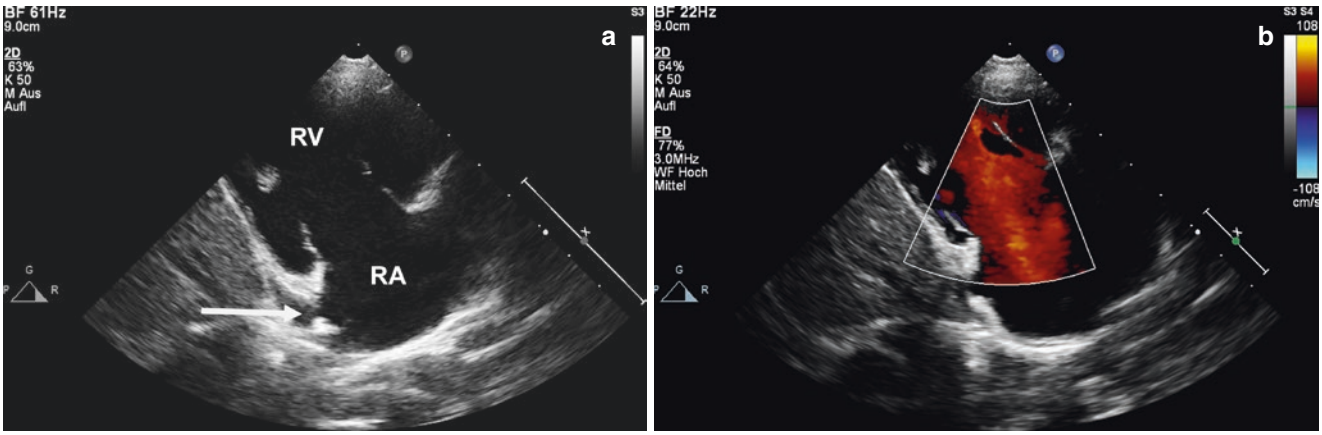

Fig. 1.4 The parasternal long-axis view of the right ventricular inflow displaying right atrium (RA), right ventricle (*RV*), the coronary sinus (*arrow*) and tricuspid valve (**a**); colour Doppler shows diastolic inflow into the right ventricle (**b**)

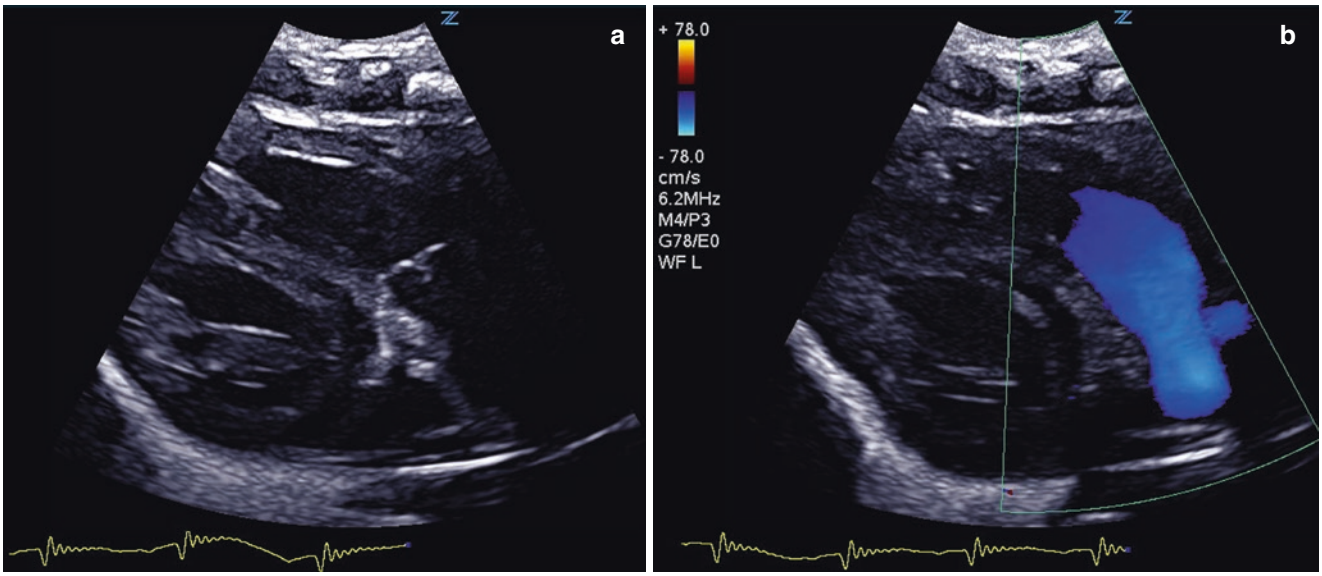

Fig. 1.5 The parasternal long-axis view of the right ventricular outflow tract shows the transition of the right ventricular outflow tract to the main pulmonary artery and the pulmonary valve (**a**); colour Doppler displays systolic flow in the main pulmonary artery in blue (**b**)

pulmonary artery (Video 1.8). This plane allows colour Doppler interrogation of the tricuspid valve, the right ventricular outflow tract and the pulmonary valve (Fig. 1.7 b, c). A sweep starting from this plane down to the apex of the heart displays the left ventricle in cross section and the different parts of the ventricular septum. Standardized planes are obtained at the level of the mitral valve leaflets and the papillary muscles (Figs. 1.8 and 1.9, Videos 1.9 and 1.10). Colour Doppler examination performed in this sweep from the base to the apex is extremely important in the search for ventricular septal defects.

Cranial tilt of the transducer starting from the plane across the base of the heart displays the left atrium and the pulmonary veins (Fig. 1.10, Video 1.11). Colour Doppler examination in this plane confirms a normal connection of the pulmonary veins to the left atrium. Pulmonary venous flow can be confirmed by pulsed wave Doppler interrogation of the different veins. Slightly cranial tilt of the transducer shows the main pulmonary artery, the pulmonary bifurcation and the right pulmonary artery in longitudinal section (Fig. 1.11. Video 1.12).

Counterclockwise rotation of the transducer in a high left parasternal position with the transducer notch at 12 o'clock displays the transition of the main pulmonary artery to the left pulmonary artery (Lai and Ko 2009). The distal aortic arch, the aortic isthmus and the proximal descending aorta

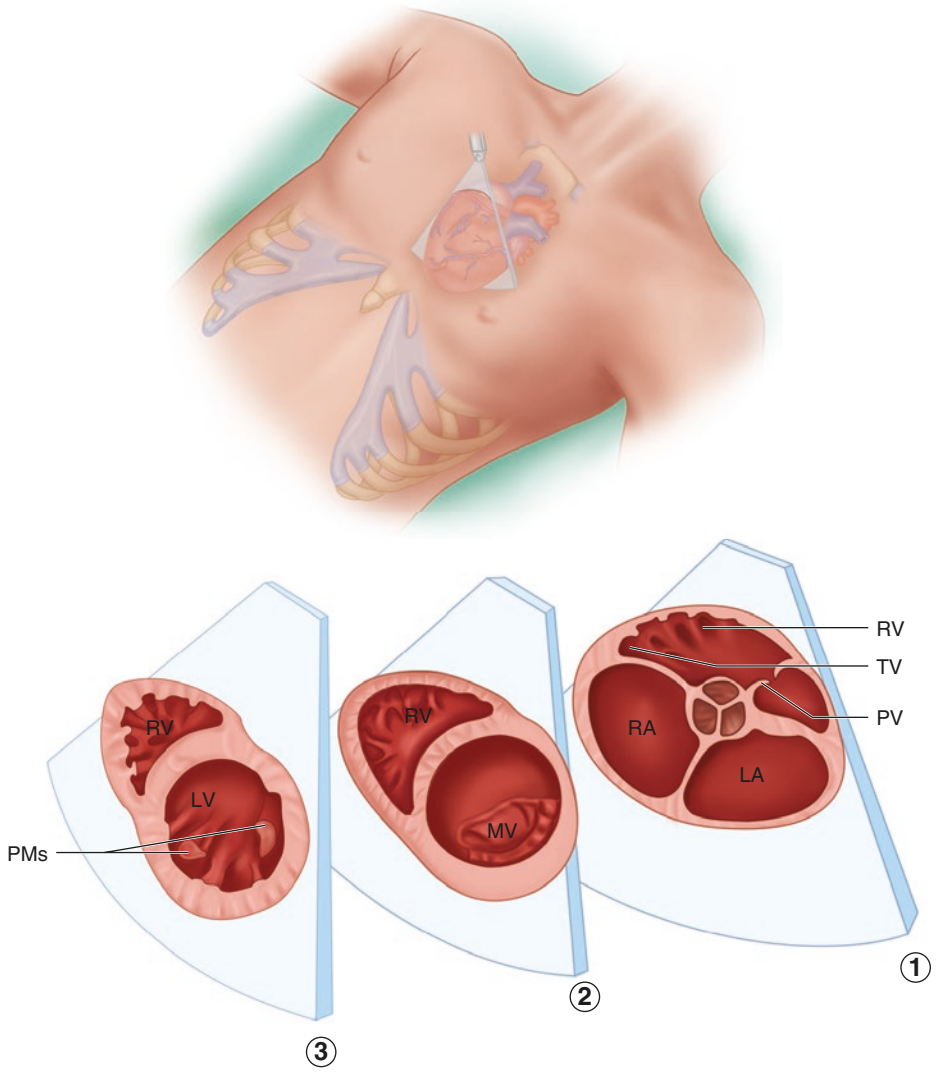

Fig. 1.6 Diagram displaying the parasternal short-axis views of the base of the heart *1*, the mitral valve *2* and the left ventricle in cross section *3*. *MV* mitral valve, *PM* papillary muscle

are displayed behind the left pulmonary artery (Fig. 1.12). On colour Doppler examination, both flow in the left pulmonary artery and in the descending aorta is directed away from the transducer and therefore displayed in blue. This plane, called "ductal view", is ideal for colour Doppler confirmation of patent ductus arteriosus, since flow entering the pulmonary artery via a patent duct is directed towards the transducer and therefore coded red (Lai and Ko 2009). Due to the favourable insonation angle, flow velocities across the ductus can be quantified by application of pulsed or continuous wave Doppler. Beyond infancy this plane frequently requires placement of the patient in a rather steep left lateral decubitus position.

Placement of the transducer close to the sternum in the second right intercostal space displays the *right parasternal views* (Lai et al. 2006; Lai and Ko 2009). A sagittal orientation of the ultrasound beam with the notch of the transducer at 12 o'clock allows visualization of the superior caval vein and its connection to the right atrium (Fig. 1.13). The right pulmonary artery is displayed behind the caval vein in cross section. Medial tilt of the transducer shows the ascending aorta (Fig. 1.14). This plane offers a good insonation angle for evaluation of flow across the aortic valve and can be employed for PW or CW Doppler assessment of systolic flow velocities in patients with aortic valve stenosis. In older children, this is facilitated by positioning the patient in a right lateral decubitus position (Lai and Ko 2009). A 90° clockwise rotation from the right parasternal sagittal view, bringing the notch of the transducer in the position of 3 o'clock, displays the innominate vein and its connection to the caval vein

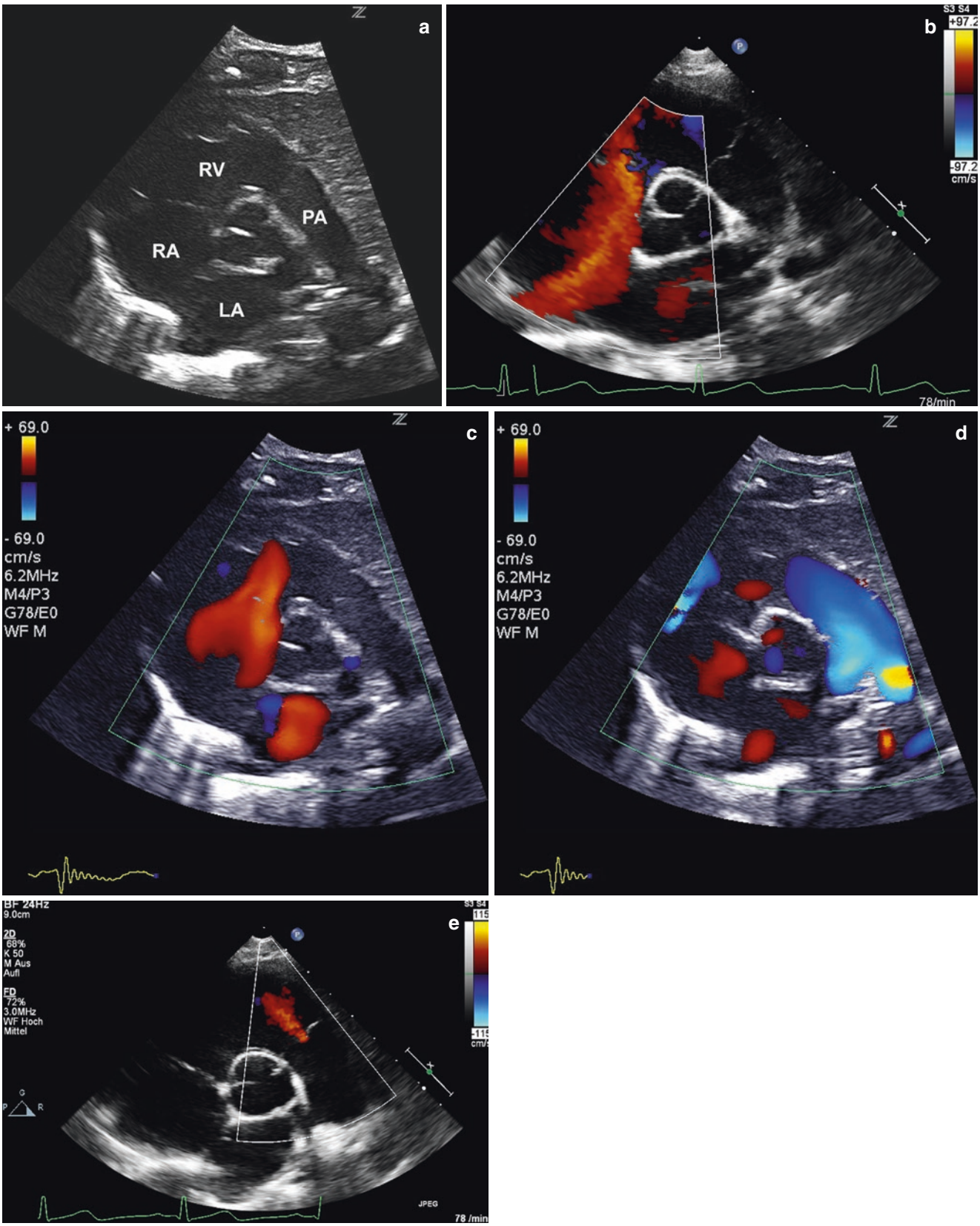

Fig. 1.7 The parasternal short axis at the base of the heart (**a**) shows the aortic valve with its three cusps in cross section, surrounded by the left atrium (*LA*), right atrium (*RA*), right ventricle (*RV*) and pulmonary artery (*PA*); colour Doppler displays venous inflow into the RA from the inferior vena cava (**b**), diastolic inflow into the right ventricle across the tricuspid valve (**c**) and systolic outflow into the main pulmonary artery (**d**). Minor pulmonary regurgitation is present in many normal children (**e**)

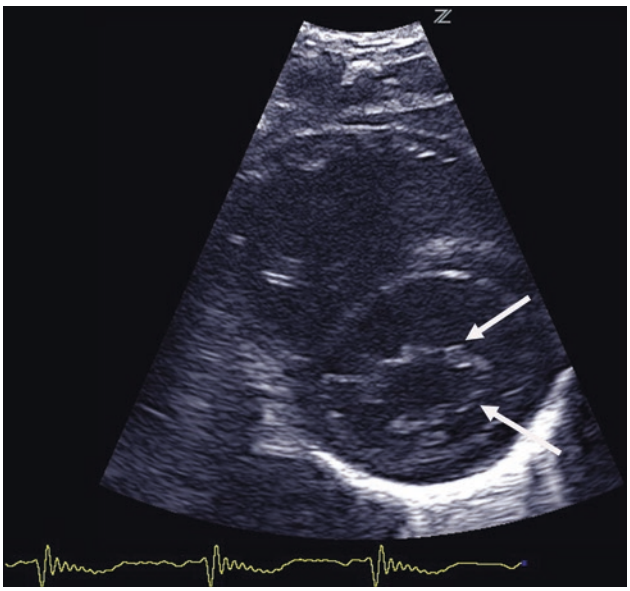

Fig. 1.8 Parasternal short axis of the left ventricle at the level of the mitral valve showing the anterior and posterior mitral valve leaflets (*arrows*)

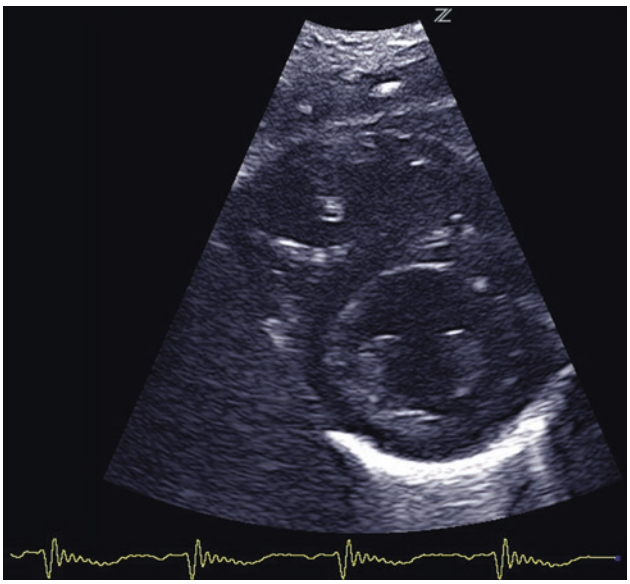

Fig. 1.9 Parasternal short axis of the left ventricle at the level of the papillary muscles

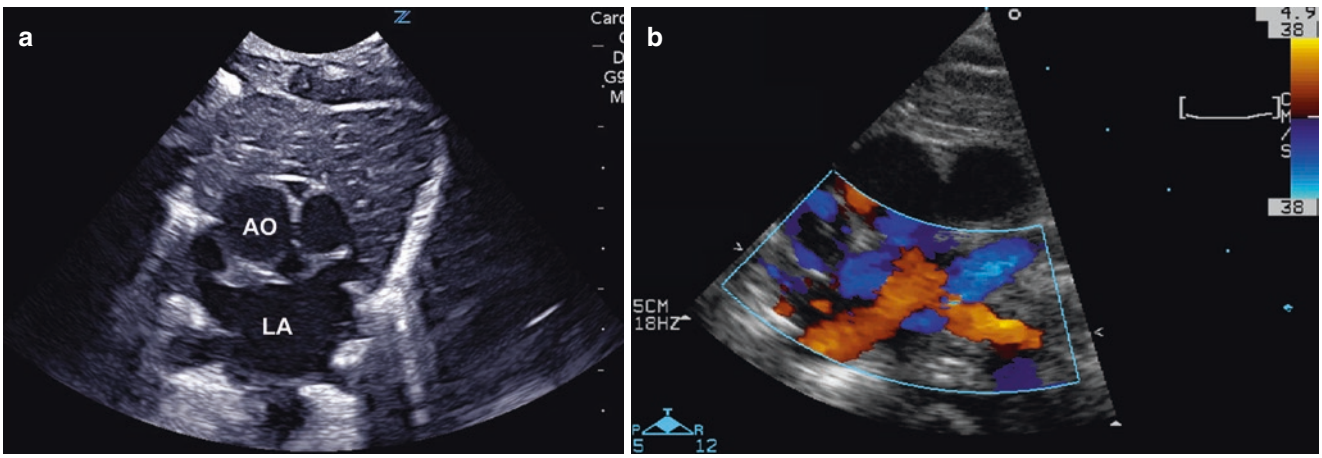

Fig. 1.10 Parasternal short axis cranial to the base of the heart (**a**) showing the left atrium (*LA*) and the pulmonary veins behind the aorta (*AO*). Colour Doppler in this view shows both upper and lower pulmonary veins entering the left atrium (**b**)

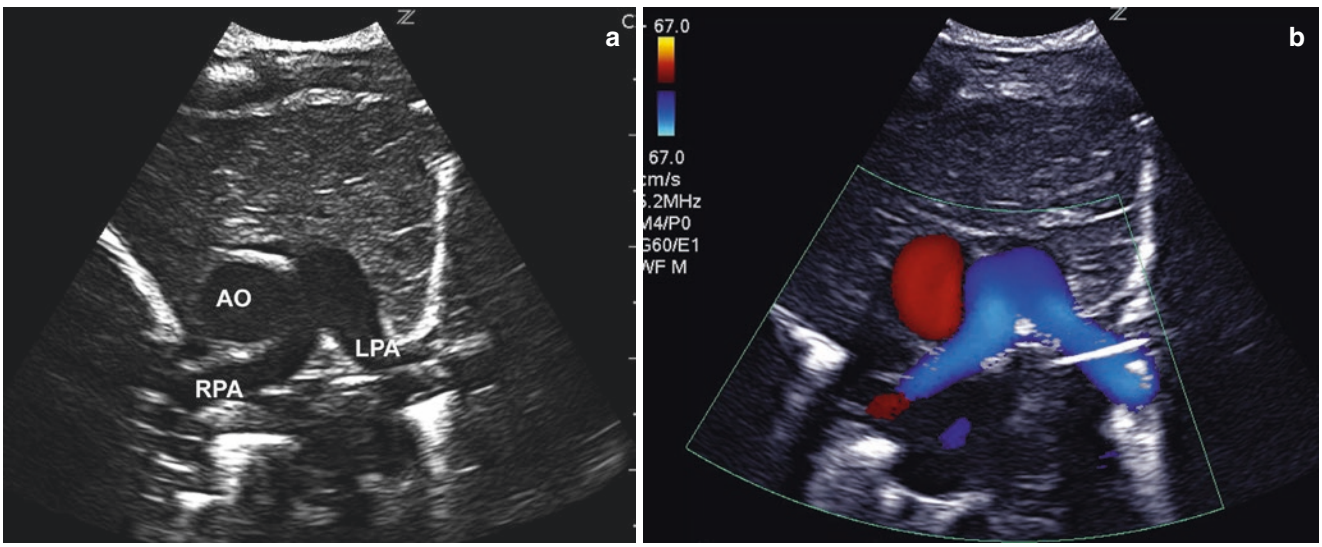

Fig. 1.11 Parasternal short axis of the pulmonary bifurcation depicting the aorta (*AO*) in cross section and right (*RPA*) and left (*LPA*) pulmonary artery (**a**); colour Doppler reveals systolic flow to both pulmonary arteries (**b**)

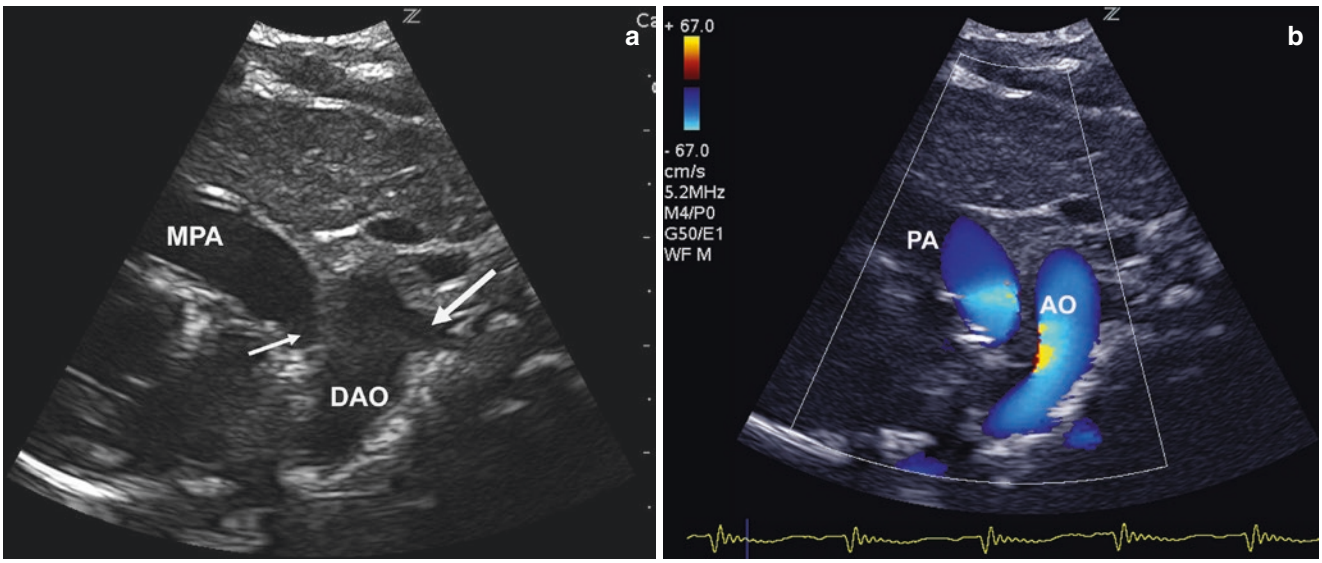

Fig. 1.12 "Ductal view" obtained from a high left parasternal window (**a**) displaying the main pulmonary artery (*PA*) with its transition into the left pulmonary artery (*small arrow*) and the distal aortic arch (*DAO*) with the left subclavian artery (*large arrow*). Colour Doppler in the ductal view reveals antegrade flow to the left pulmonary artery and in the distal aortic arch (**b**)

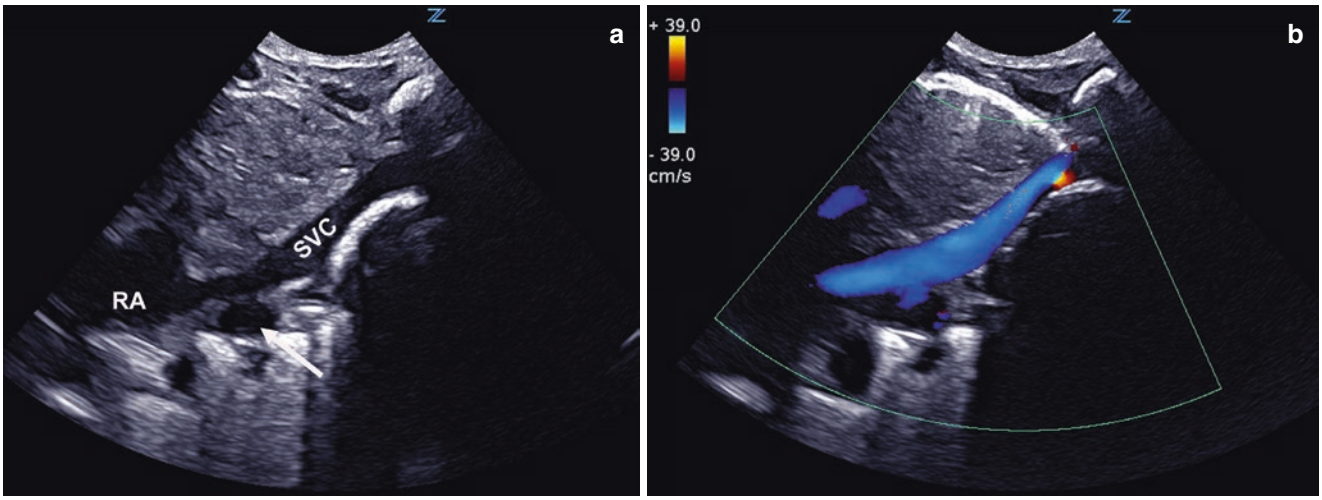

Fig. 1.13 The high right parasternal longitudinal view (**a**) shows the superior vena cava (*SVC*) draining into the right atrium (*RA*) with its course anterior to the right pulmonary artery, which is displayed in cross section (*arrow*); colour Doppler displays flow in the vena cava (**b**)

(Fig. 1.15). A caudal sweep displays the right pulmonary artery in longitudinal section, the right pulmonary vein and its connection to the left atrium (Lai and Ko 2009).

1.2.2 Apical Views

The *apical four-chamber views* are obtained by placement of the transducer directly over the cardiac apex (Lai et al. 2006; Lai and Ko 2009; Snider et al. 1997), which is usually located below the left mamilla. The transducer is nearly oriented in a coronal plane with the notch pointing towards the left axilla (Fig. 1.16). While the apical planes can be obtained in infants in the supine position, in children older than 2–3 years of age, it is favourable to place the child in a left decubitus position with elevation of the left arm to approximate the heart to the left chest wall (Lai and Ko 2009; Snider et al. 1997). The standard plane of the apical four-chamber view displays both atria and ventricles, the atrioventricular valves and the insertion of their leaflets, as well as the moderator band and apical trabeculation of the right ventricle (Fig. 1.17, Video 1.13). Ventricular and atrial septum should be displayed in the centre of the screen and should be

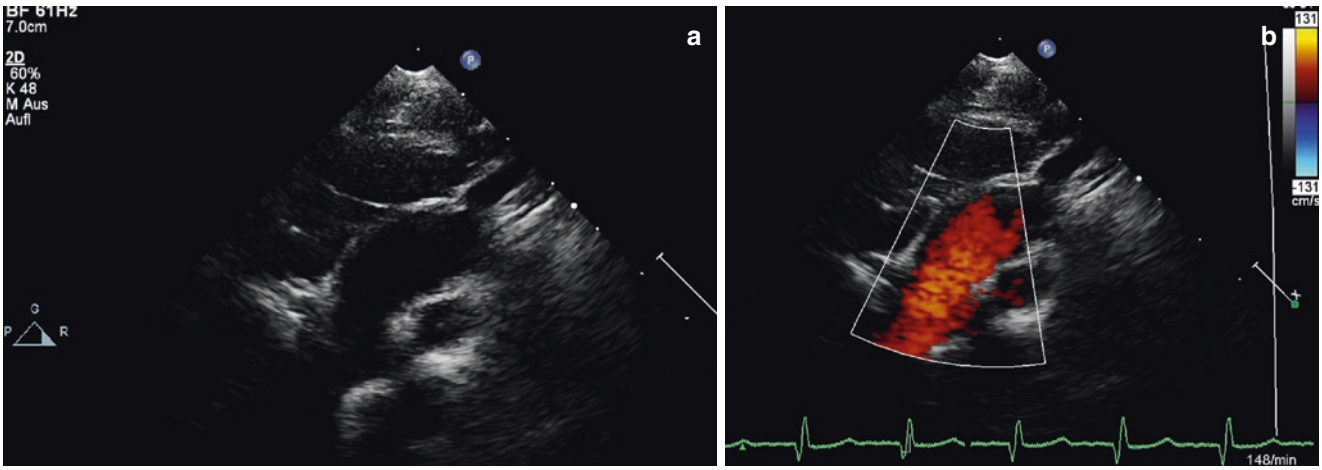

Fig. 1.14 Right parasternal short axis view of the ascending aorta (**a**); systolic flow in the ascending aorta (*AO*) is directed towards the transducer and coded in red (**b**)

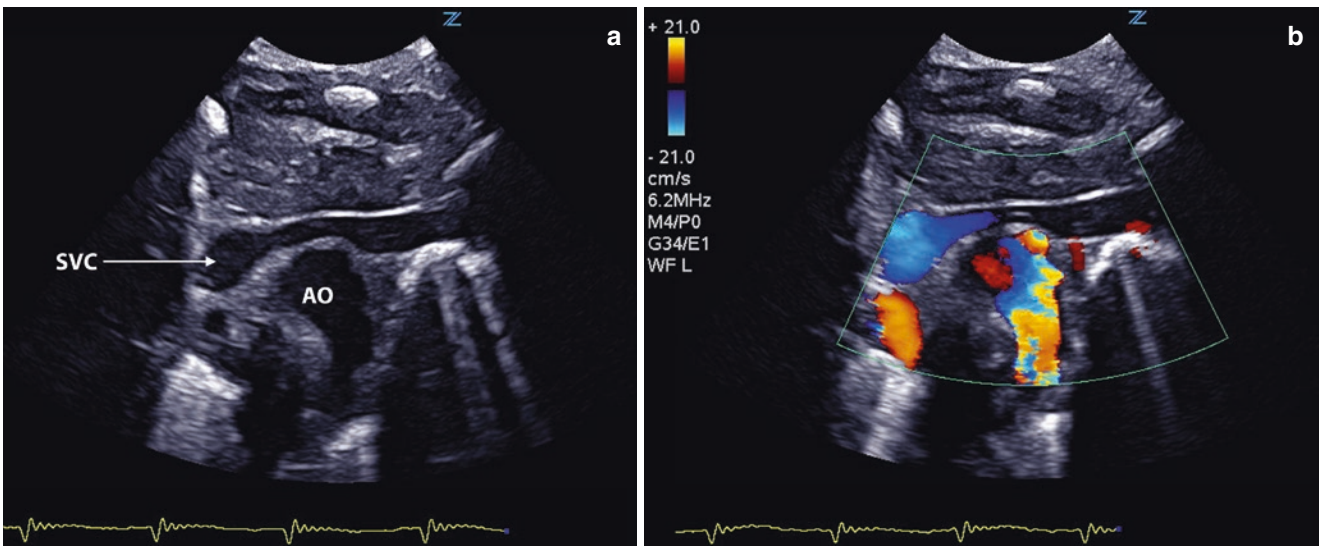

Fig. 1.15 High right parasternal short axis view (**a**) depicting the innominate vein superior to the aorta (*AO*) on its way to the superior vena cava (*SVC*); on colour Doppler, flow in the superior vena cava, directed from the transducer, is coded blue (**b**)

aligned parallel to the ultrasound beam. Posterior tilt of the transducer displays the muscular inlet septum and the coronary sinus coursing in the atrioventricular groove to the right atrium (Fig. 1.18, Video 1.14). Anterior tilt of the transducer shows a plane that is also termed "apical five-chamber view", visualizing the perimembranous ventricular septum, the left ventricular outflow tract and the aortic valve (Fig. 1.19, Video 1.15). The apical four-chamber view is the ideal plane for colour Doppler interrogation of both atrioventricular valves, since flow across the valves is directed towards the transducer (Fig. 1.17). In addition it offers optimal conditions for PW and CW Doppler quantification of diastolic inflow and systolic regurgitant flow in the presence of tricuspid and mitral regurgitation. Colour Doppler interrogation of the ventricular septum in the standard and in the posterior plane helps to detect defects in the apical and in the inlet parts of the muscular ventricular septum. The anterior plane ("apical five-chamber view") allows colour Doppler assessment of the left ventricular outflow tract and the aortic valve (Fig. 1.19, Video 1.15). Aortic regurgitation can be detected and quantified according to its extension back into the left ventricle. This plane is also important for interrogation of flow in the left ventricular outflow tract by pulsed or continuous wave Doppler especially in the presence of subaortic obstruction.

Fig. 1.16 Diagram depicting the planes of the apical four-chamber view including the posterior *1*, medial *2* and anterior plane *3*. *CS* coronary sinus

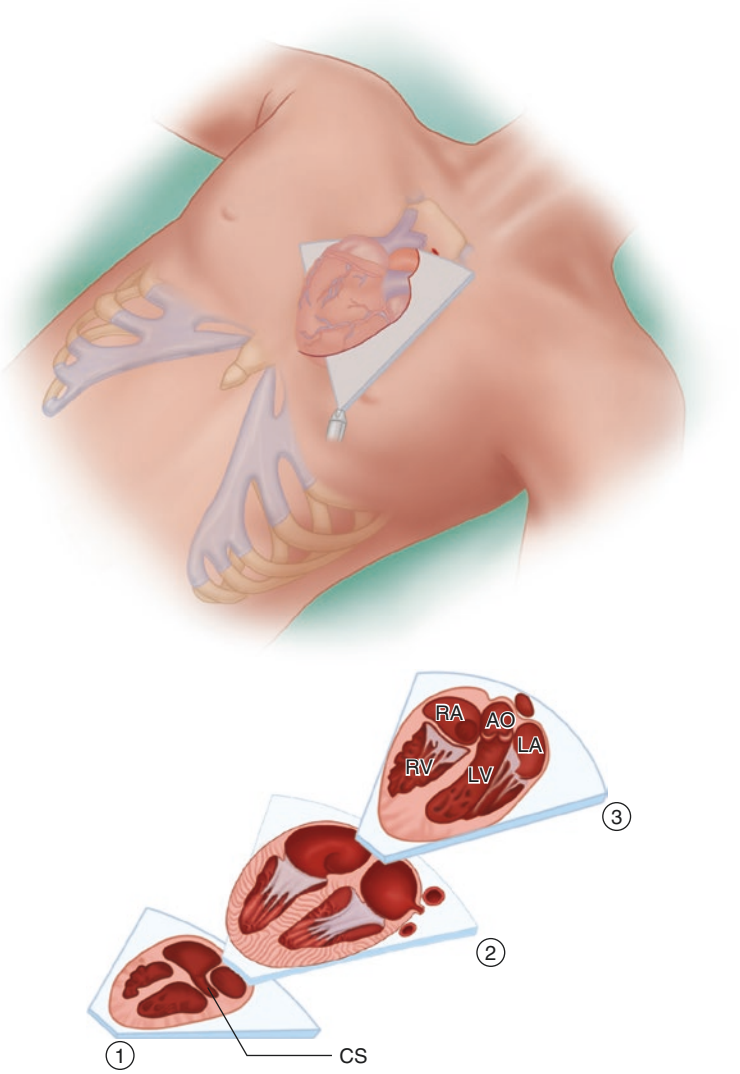

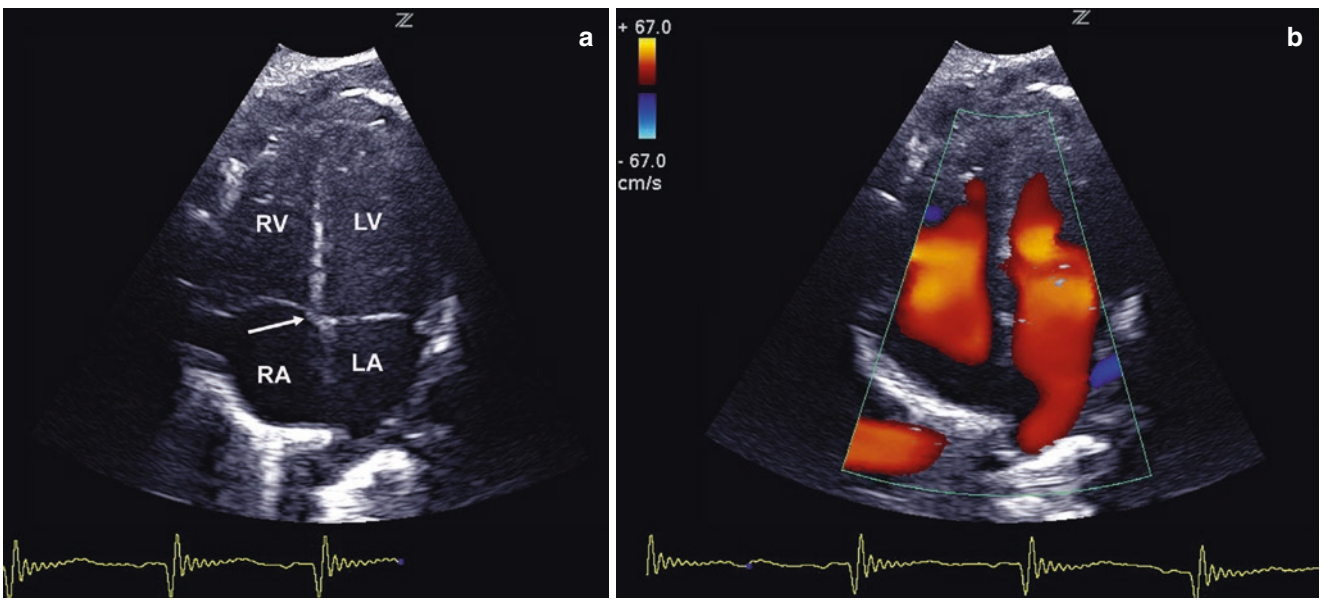

Fig. 1.17 The apical four-chamber view (**a**) visualizes both ventricles (*LV*, *RV*) and atria (*LA*, *RA*); the right ventricle is characterized by septal insertion of the tricuspid valve that is closer to the apex than the mitral insertion (*arrow*). The right ventricular apex is characterized by a septo-parietal moderator band and is more trabeculated than the left. Colour Doppler shows diastolic inflow directed towards the transducer (**b**)

1.2.3 Subcostal Views

Subcostal imaging starts with a transverse section of the upper abdomen to determine the position of the inferior caval vein and of the abdominal aorta (Lai et al. 2006, Lai and Ko 2009; Mertens et al. 2010; Tacy and Silverman 2001). In patients with situs solitus, the inferior caval vein is located to the right and the aorta to the left of the spine (Fig. 1.20, Video 1.16). Clockwise rotation of the probe for 90°, bringing the transducer notch to the 6 o'clock position, allows longitudinal visualization of these vessels (Fig. 1.21). Colour Doppler examination of the abdominal aorta in this plane displays the origin of the coeliac and upper mesenteric artery and provides the basis for pulsed wave interrogation of flow in these systemic arteries (Fig. 1.22). Since flow in the coeliac artery is directed towards the transducer, PW Doppler can be used for semiquantitative assessment of blood flow in the systemic circulation and will detect diminished systolic flow in the presence of critical coarctation and decreased or even negative diastolic flow in the presence of significant diastolic run-off from the aorta. The latter can be expected in the presence of severe aortic regurgitation, in neonates with truncus arteriosus communis or in the presence of a large ductus arteriosus or an aortopulmonary window.

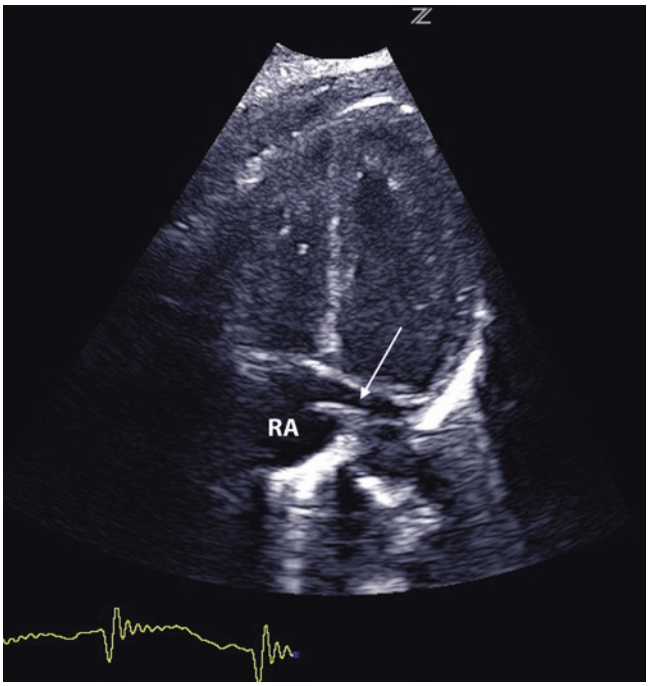

Fig. 1.18 The posterior plane of the apical four-chamber shows inferior parts of the muscular ventricular septum and the coronary sinus (*arrow*) coursing in the atrioventricular groove to the right atrium (*RA*)

Cranial tilt of the transducer from the transverse section of the abdomen shows the connection of the inferior caval vein with the right atrium. The hepatic veins join the right atrium just proximal to the right atrium. Subcostal examination of the heart includes coronal, sagittal and oblique views. For subcostal imaging, it is generally recommended to invert the imaging plane to display superior structures at the top of the image (Lai et al. 2006). The *subcostal long-axis* (*coronal*) *views* are obtained by placement of the transducer in the abdomen underneath and parallel to the sternum with an orientation of the ultrasound beam from right to left and the transducer notch in the 3 o'clock position (Snider et al. 1997). A series of planes can be obtained by tilting the transducer from a posterior to an anterior position (Fig. 1.23, Video 1.17). The posterior coronal view displays both atria

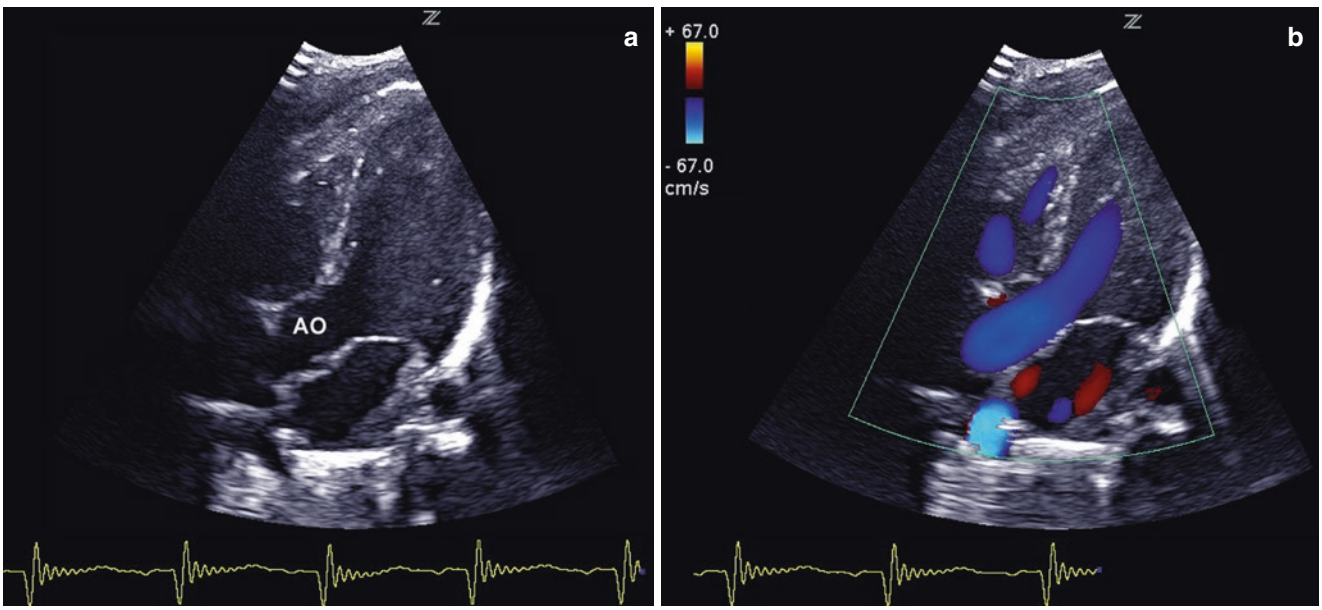

Fig. 1.19 The anterior plane of the apical four-chamber view (**a**) displays the left ventricular outflow tract and the aorta (*AO*); colour Doppler shows systolic flow from the left ventricle to the aorta (**b**)

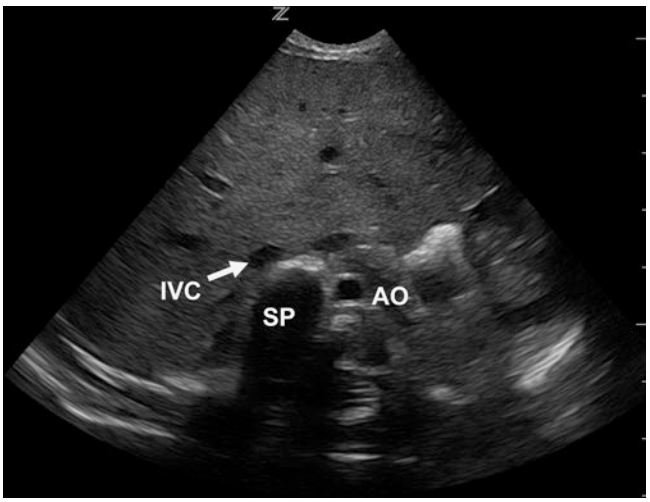

Fig. 1.20 The cross section of the great vessels in the upper abdomen shows the inferior vena cava (*IVC*) to the right and the abdominal aorta (*AO*) to the left of the spine (*SP*)

and the drainage of the superior pulmonary veins into the left atrium, which can be confirmed by colour Doppler examination (Fig. 1.24, Video 1.18). Anterior tilt of the transducer shows the left ventricle, parts of the ventricular septum, the left ventricular outflow tract and the aortic valve (Fig. 1.25). This coronal plane is very useful for colour Doppler examination of the left ventricular outflow tract and the aortic valve. Due to the favourable insonation angle, it offers the possibility for quantification of systolic flow across the aortic valve by pulsed and continuous wave Doppler. Further anterior tilt opens the right ventricle and the right ventricular outflow tract (Fig. 1.26, Video 1.19). This plane is especially helpful for colour Doppler interrogation of the right ventricular outflow tract and for detection of subvalvular obstruction (Video 1.20), which can be quantified by PW and CW Doppler assessment.

A 90° clockwise rotation of the transducer from the coronal planes, bringing the notch of the transducer into the

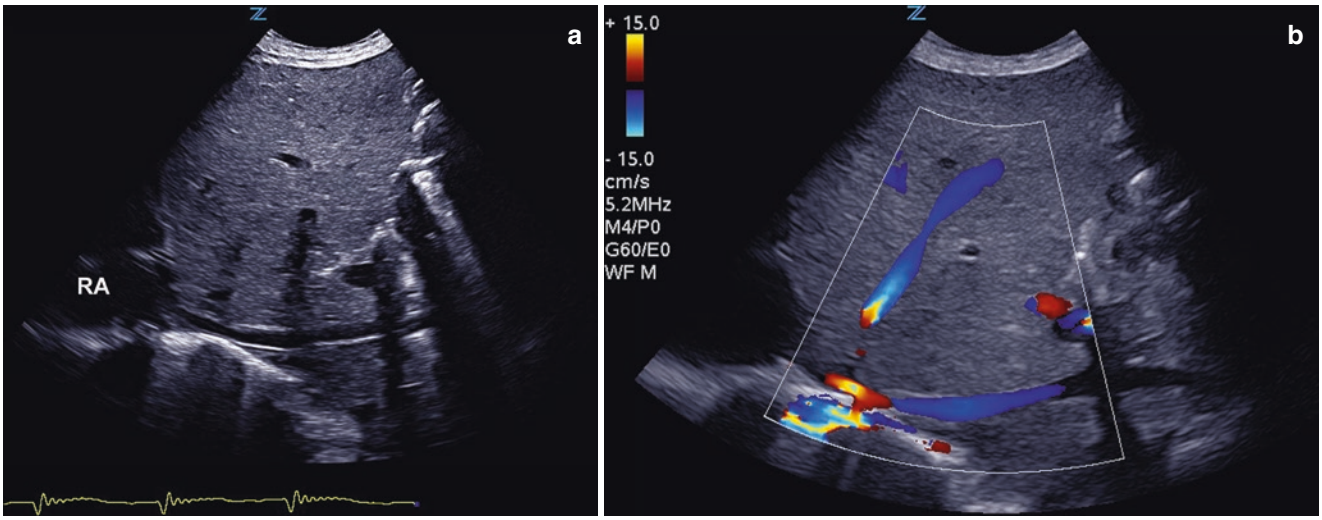

Fig. 1.21 Longitudinal view (**a**) and colour Doppler of the inferior vena cava (**b**) on its way to the right atrium (RA)

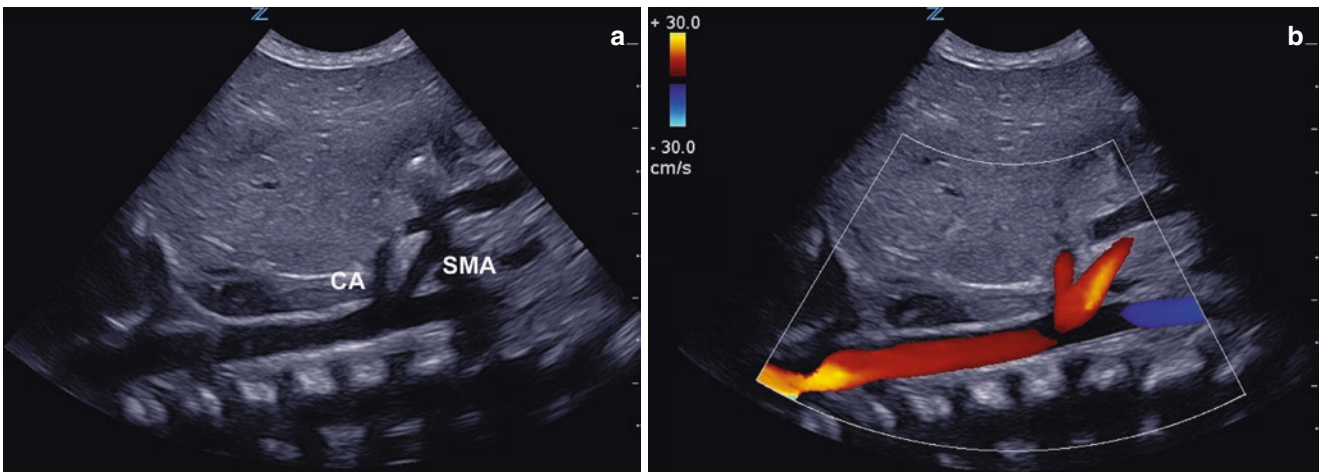

Fig. 1.22 Longitudinal view of the abdominal aorta (**a**) showing the origin of the coeliac (*CA*) and superior mesenteric artery (*SMA*), which are well displayed by colour Doppler (*b*)

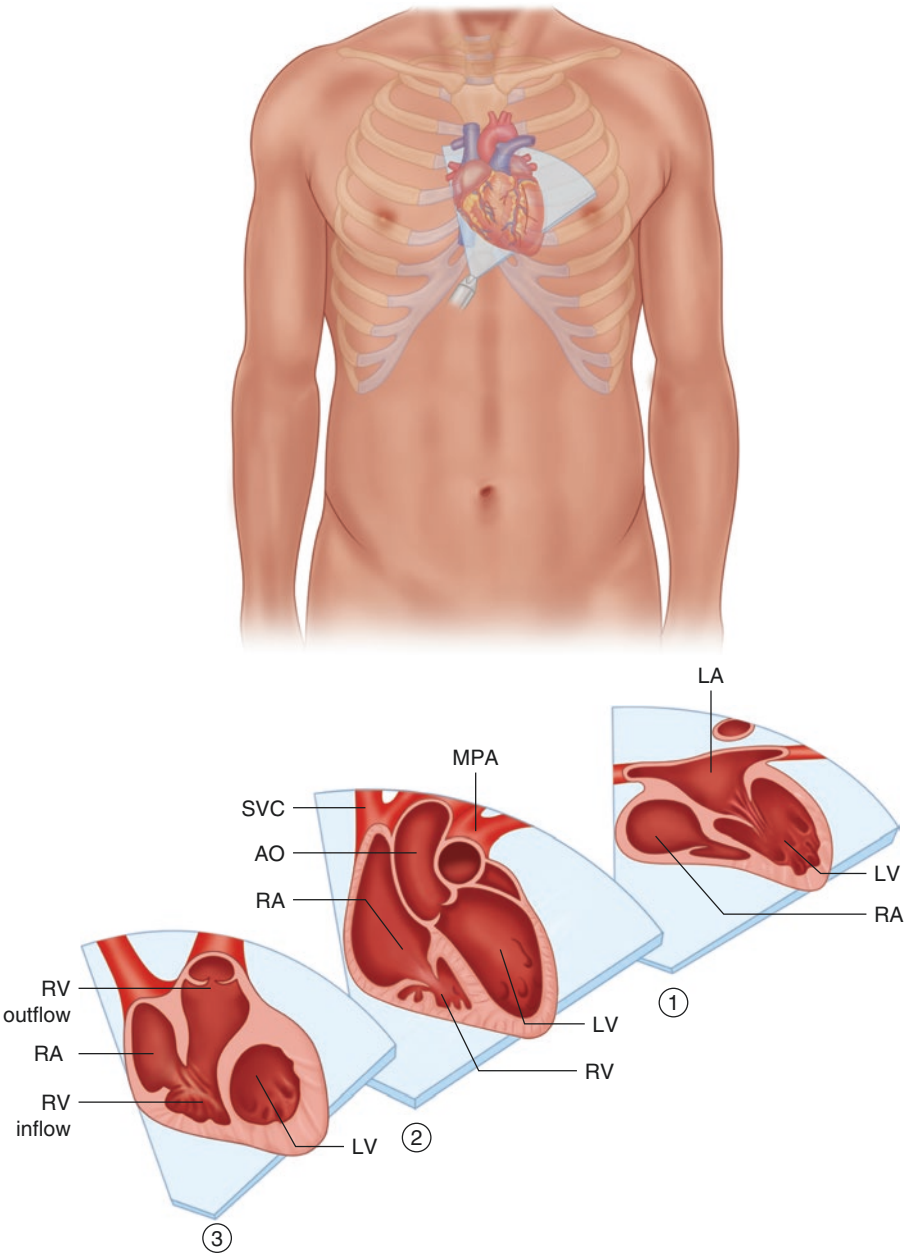

Fig. 1.23 Diagram of the subcostal coronal (long-axis) views starting with the posterior plane of the atria *1*, the medial plane of the left ventricular outflow tract *2* and the anterior plane of the right ventricular outflow tract *3*. *SVC* superior vena cava, *RV* right ventricle

6 o'clock position, displays the *subcostal short-axis* (*sagittal*) *views* (Lai et al. 2006; Snider et al. 1997) (Video 1.21). The most rightward of these planes shows the drainage of the superior and inferior caval veins into the right atrium (Fig. 1.27, Video 1.22). Furthermore this plane depicts the cranial part of the atrial septum (Fig. 1.28). Slight counterclockwise rotation in this plane results in a left oblique view with very nice elongation of the interatrial septum. Back in the sagittal plane, leftward sweep of the transducer reveals the sagittal plane of the right ventricular outflow tract (Fig 1.29, Video 1.23). It displays the infundibulum of the right ventricle, the pulmonary valve and the main pulmonary artery. This plane allows Doppler interrogation of the right ventricular outflow tract and the pulmonary valve. Further leftward tilt of the transducer towards the left shoulder shows the left ventricle in cross section (Fig. 1.30, Video 1.24).

The *subcostal RAO view* is an additional plane which is obtained by counterclockwise rotation of the transducer starting from a subcostal long-axis view (Lai and Ko 2009). It displays the tricuspid valve, the right ventricle and its infundibulum as well as the pulmonary valve and the main pulmonary artery (Fig. 1.31). This plane resembles the para-

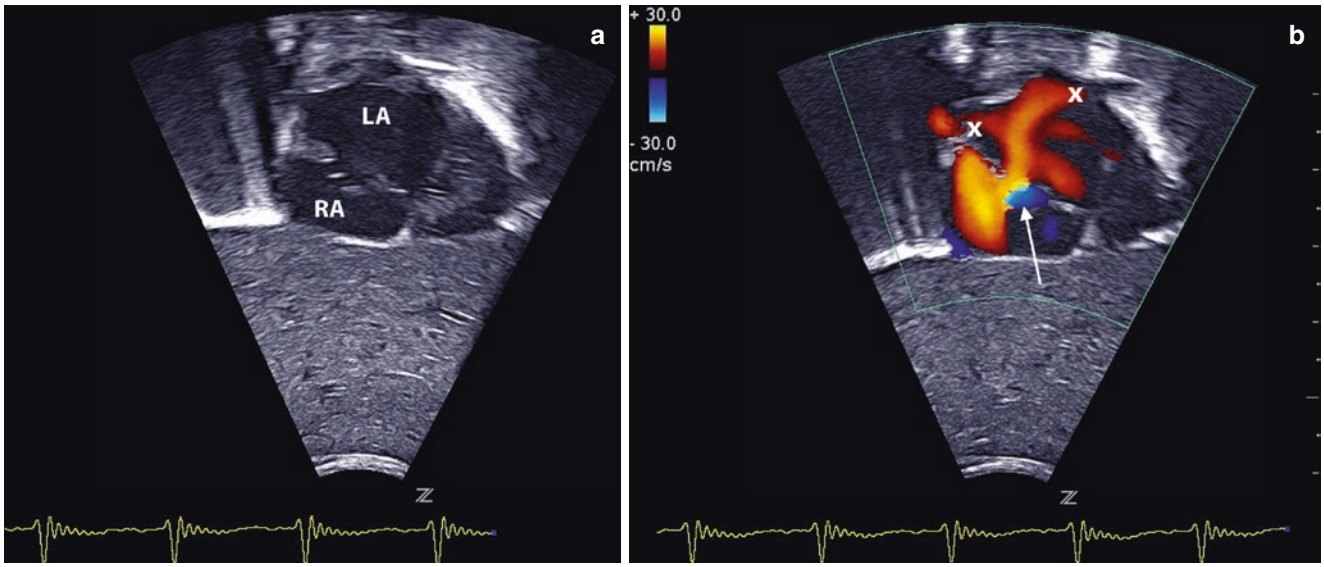

Fig. 1.24 Posterior subcostal coronal view of the atria (**a**) showing the left (*LA*) and right atrium (*RA*) as well as the atrial septum. Flow from both upper pulmonary veins (*x*) is apparent on colour Doppler (**b**); in this neonate there is still flow across a small patent foramen ovale (*arrow*)

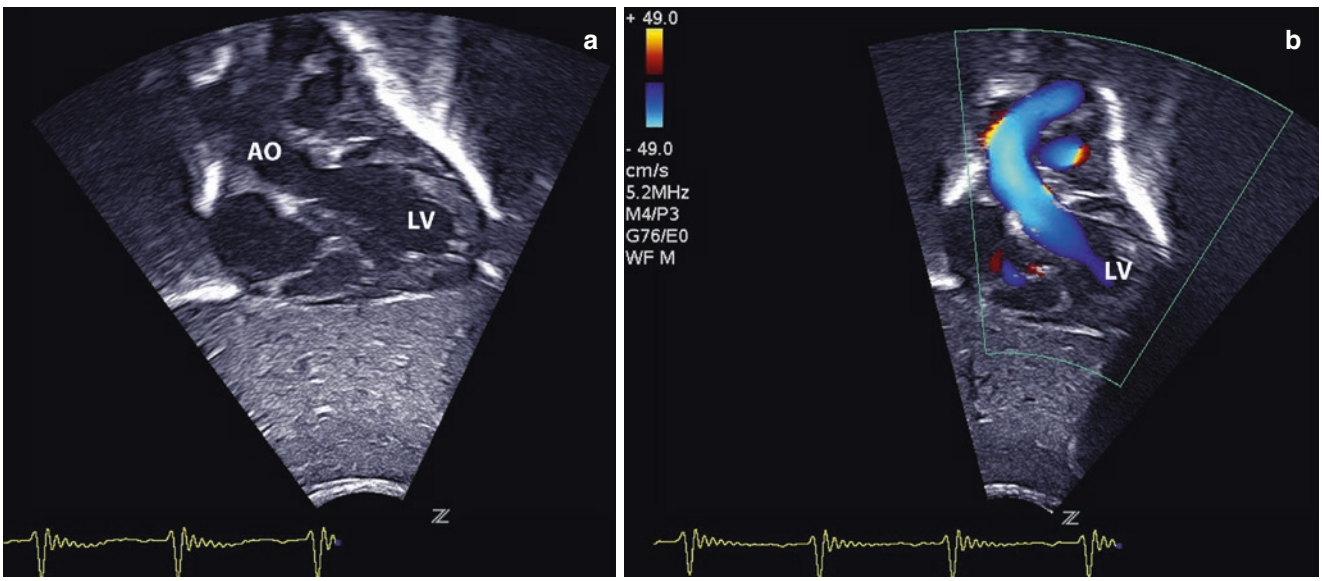

Fig. 1.25 Subcostal coronal view of the left ventricular outflow tract (**a**); colour Doppler (**b**) shows systolic flow from the left ventricle (*LV*) to the aorta (*AO*)

sternal short axis view with the aortic valve in cross section in the centre of the image. It allows CD interrogation of the perimembranous ventricular septum, of the right ventricular outflow tract and of the pulmonary valve (Fig. 1.31).

1.2.4 Suprasternal Views

The suprasternal views are obtained by placement of the transducer in the suprasternal notch. In neonates and young infants, the thymus gland enlarges the acoustic window, and similar views may be obtained from a high right parasternal window. Echocardiographic examination of these planes is greatly enhanced by elevation of the patient's shoulders by a towel or pillow (Lai and Ko 2009).

The *suprasternal short-axis* view displays the ascending aorta in cross section (Fig. 1.32, Video 1.25). The innominate vein is depicted superior to the aorta while the right pulmonary artery and the left atrium are displayed

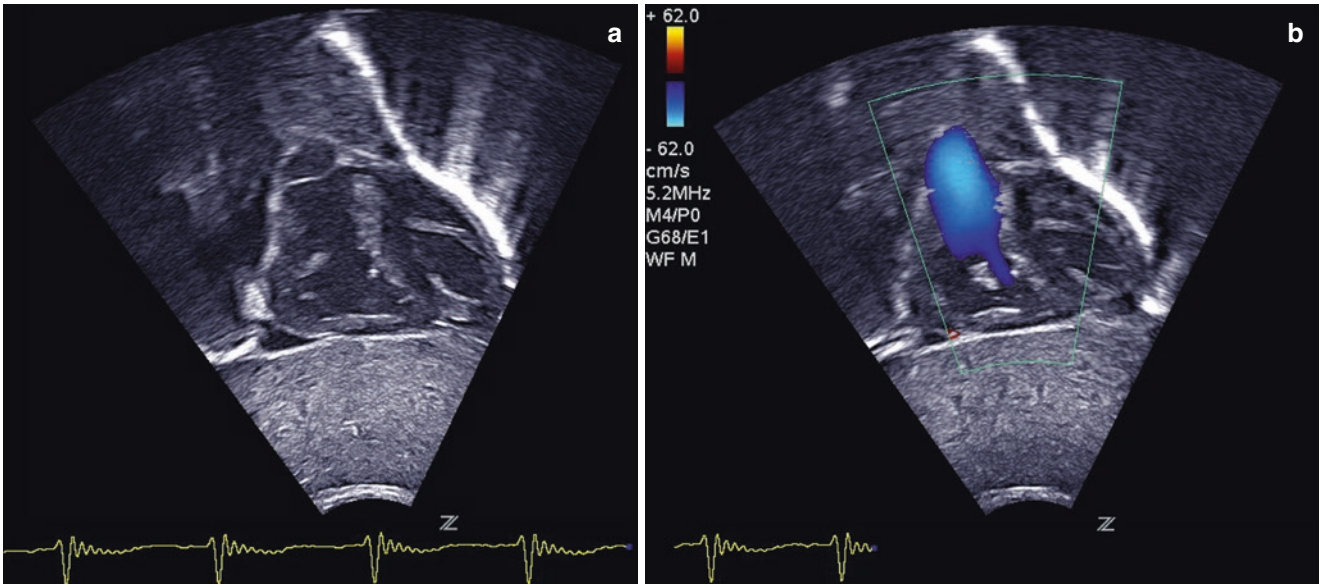

Fig. 1.26 Subcostal coronal view of the right ventricular outflow tract (**a**) and colour Doppler confirmation of systolic flow to the pulmonary artery (**b**)

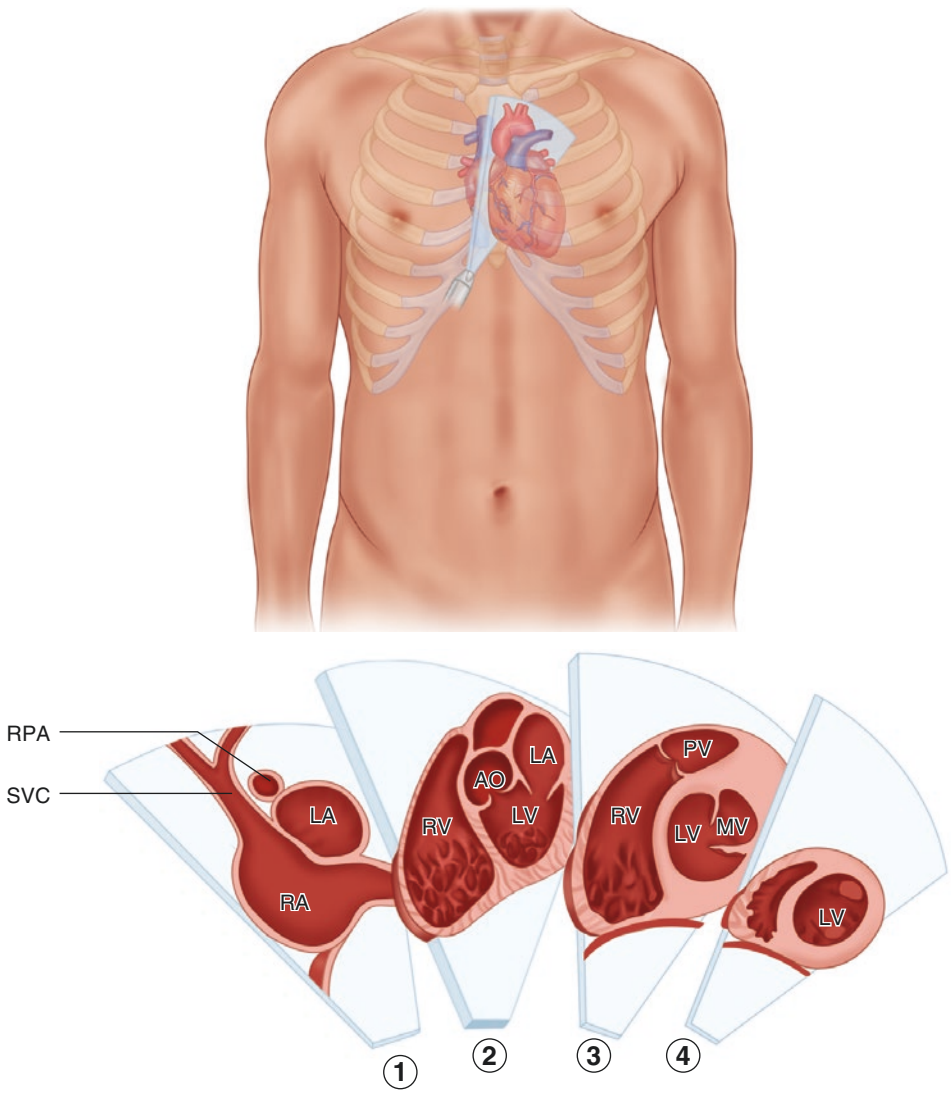

Fig. 1.27 Diagram of the subcostal short-axis (sagittal) views including from right to left the plane of the caval veins *1*, followed by the planes of the right ventricular outflow tract *2, 3* and finally the cross section of the left ventricle *4*. *SVC* superior vena cava, *RPA* right pulmonary artery, *RV* right ventricle, *LV* left ventricle, *MV* mitral valve, *PV* pulmonary valve

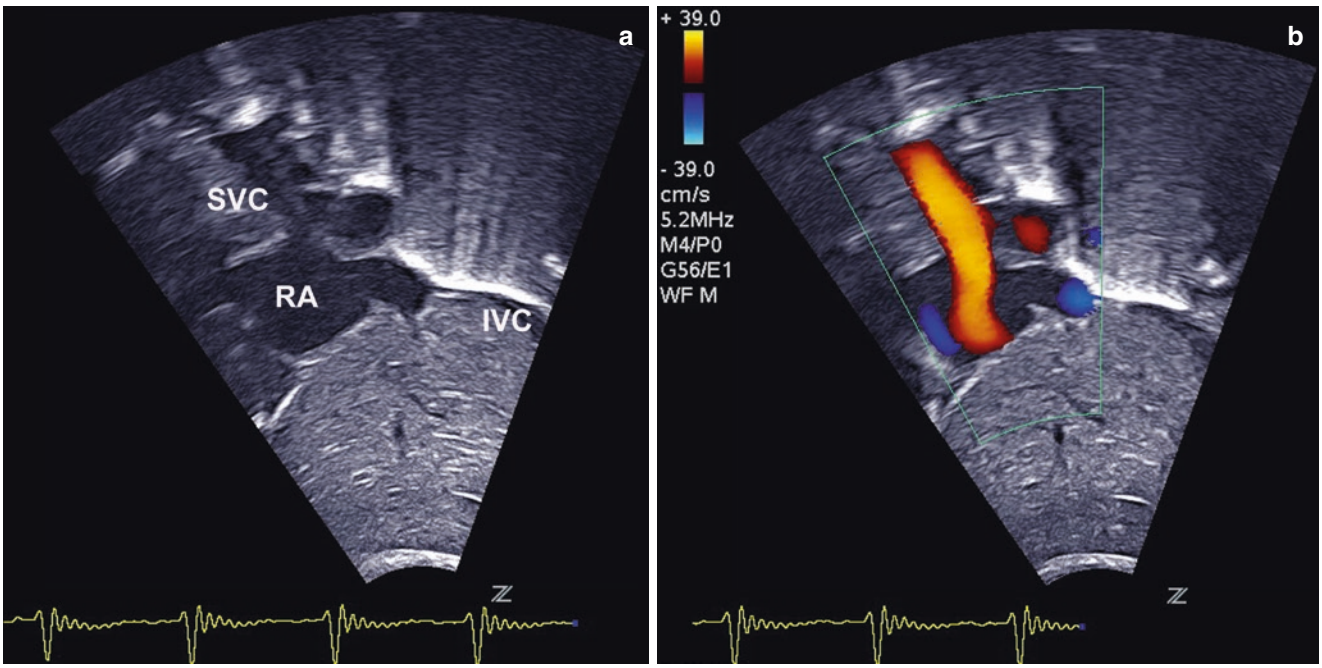

Fig. 1.28 Subcostal short-axis view of the caval veins (**a**) showing the superior (*SVC*) and inferior vena cava (*IVC*) entering the right atrium (*RA*) with confirmation of flow by colour Doppler (**b**)

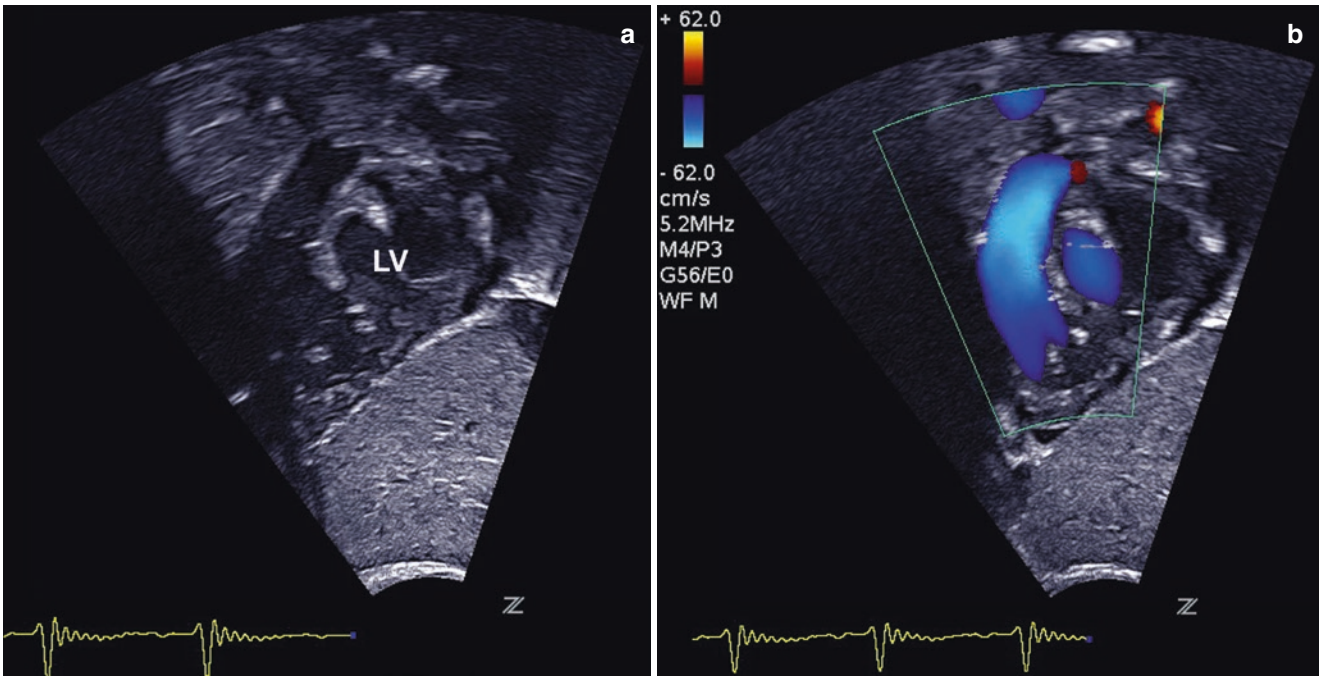

Fig. 1.29 Subcostal short-axis view of the right ventricular outflow tract and pulmonary valve (**a**). The left ventricle is displayed in cross section (*LV*). Colour Doppler depicts systolic flow from the right ventricle to pulmonary artery (**b**)

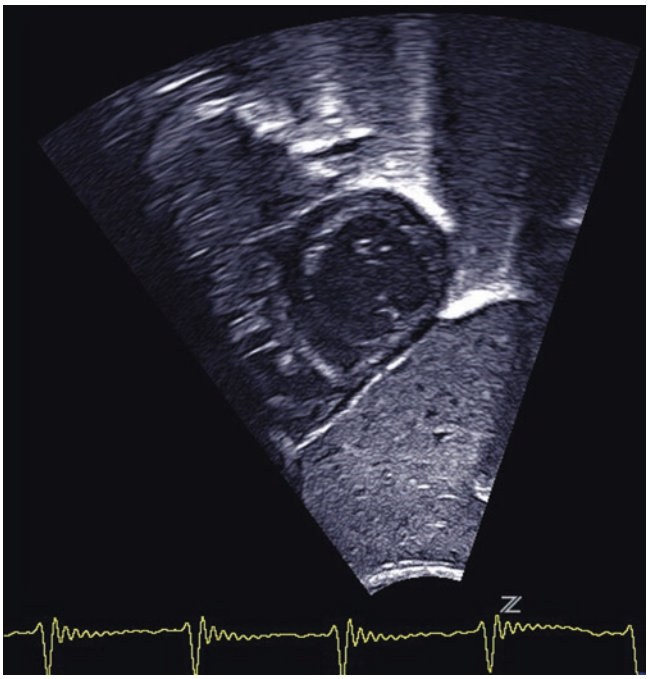

Fig. 1.30 Further leftward tilt results in the subcostal short-axis view of the left ventricle

below (Fig. 1.33). Cranial angulation of the transducer allows visualization of the brachiocephalic arteries (Videos 1.26 and 1.27). In the presence of a normal left aortic arch, the first vessel originating from the aorta will be the right innominate artery. This vessel can be opened and displayed in longitudinal section by clockwise rotation of the transducer (Fig. 1.33, Video 1.26 and 1.27). Visualization of the normal bifurcation into the right subclavian and right common carotid artery confirms the presence of a left aortic arch and excludes possible anomalies of the right subclavian artery, e.g. aberrant origin from the descending aorta (Lai and Ko 2009; Murdison et al. 1996; Snider et al. 1996). In the presence of a left aortic arch, counterclockwise rotation of the transducer starting from the suprasternal short axis opens the aorta and displays a longitudinal section of the entire aortic arch (Fig. 1.34, Video 1.28). This *suprasternal long-axis* view provides excellent conditions for colour Doppler examination of the aortic arch (Video 1.29). CDE helps to define whether there is antegrade or retrograde flow in different parts of the aortic arch, which is of special importance in the evaluation of neonates with left-sided obstructive lesions. However exact assessment of direction and timing of flow requires the application of pulsed wave Doppler interrogation. Quantification of significantly accelerated flow in the presence of severe aortic coarctation requires the application of continuous wave Doppler. It should be kept in mind, however, that circumscribed distal obstructions of the aortic isthmus may be missed in this plane. Furthermore visualization of a patent ductus arteriosus will not always be possible in this plane. *Therefore evaluation of the distal aortic arch and isthmic region should always include application of the ductal view* (Fig 1.12).

1.3 Pulsed Wave and Continuous Wave Doppler

1.3.1 Systemic Veins

Normal flow in the superior and inferior vena cave is characterized by a triphasic flow pattern (Mertens et al. 2010; Meyer et al. 1993; Reynolds and Appleton 1991; Snider et al. 1997). Systolic forward flow due to atrial relaxation and descent of the tricuspid annulus is termed S wave, while forward flow during diastole corresponding to opening of the tricuspid valve and rapid ventricular filling is termed D wave (Fig. 1.35). The A wave represents short duration retrograde flow that may occur in the caval veins towards the end of the diastole associated with atrial contraction. Flow velocities in the caval veins are influenced by respirations with a significant increase of flow velocities during inspiration. Tricuspid regurgitation results in a decrease of S wave and increase of D wave; during tachycardia S wave and D wave may merge to one peak (Snider et al. 1997). Hepatic venous flow is similar to caval venous flow except for lower flow velocities. In addition flow reversal during atrial systole is more common (81 %) in the hepatic veins (Meyer et al. 1993).

1.3.2 Tricuspid Valve

Doppler interrogation of the tricuspid valve can be performed in the apical four-chamber view, in the parasternal long axis of the right ventricular inflow and in the parasternal short axis (Fig. 1.36). Forward flow across the valve occurs during diastole with a first peak called E

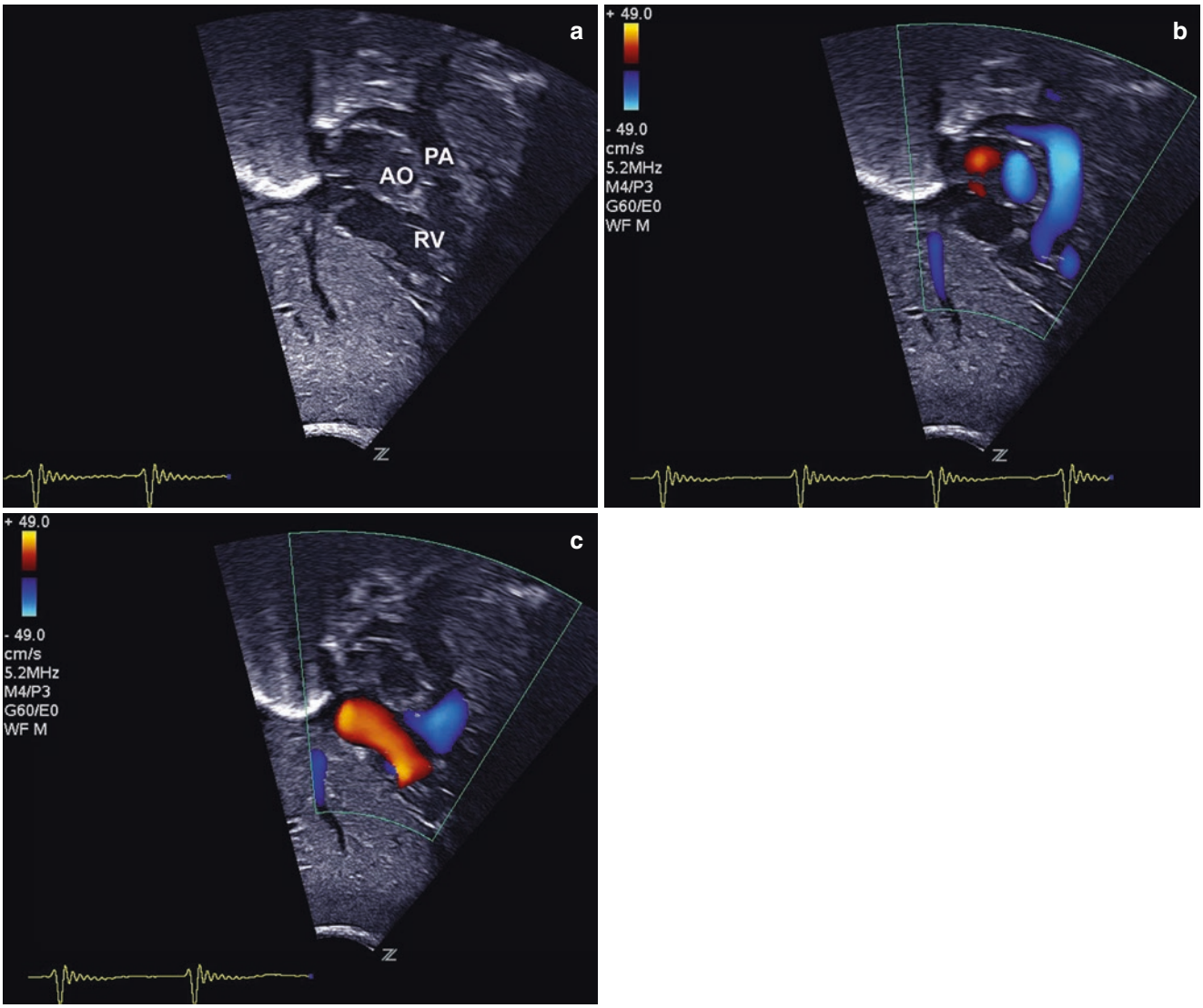

Fig. 1.31 The subcostal right anterior oblique view displays both right ventricular inflow and outflow with the aorta (*AO*) in the centre displayed in cross section (**a**); colour Doppler in systole (**b**) displays flow from the right ventricle (*RV*) to the pulmonary artery (*PA*), while the diastolic frame shows inflow from the right atrium (**c**)

wave, associated with rapid ventricular filling, and a second peak called A wave associated with atrial contraction (Mertens et al. 2010; Snider et al. 1997). While in the fetus and in the normal neonate the A wave exceeds the E wave, in infants and children, the ratio is inverted with dominance of the E wave (Snider et al. 1997). The different inflow pattern in the fetus and neonate is attributed to immaturity of ventricular myocardium with decreased compliance and dependency of ventricular filling on atrial contraction (Mertens et al. 2010; Snider et al. 1997). Normal tricuspid valve inflow velocities are lower than mitral valve velocities and show more respiratory alterations with an increase in flow velocities during inspirations.

1.3.3 Right Ventricular Outflow Tract and Pulmonary Artery

Planes for Doppler interrogation of the right ventricular outflow tract include the parasternal long axis view of the right ventricular outflow tract and the parasternal short axis and the subcostal long axis of the right ventricular outflow tract. For Doppler interrogation in the parasternal short axis, it may be favourable to position the transducer one or two intercostal spaces below the usual position to obtain optimal alignment of the Doppler beam with the outflow tract and main pulmonary artery (Snider et al. 1997). The normal peak velocity in the main pulmonary artery in children has been reported with 0.9 m/s with a

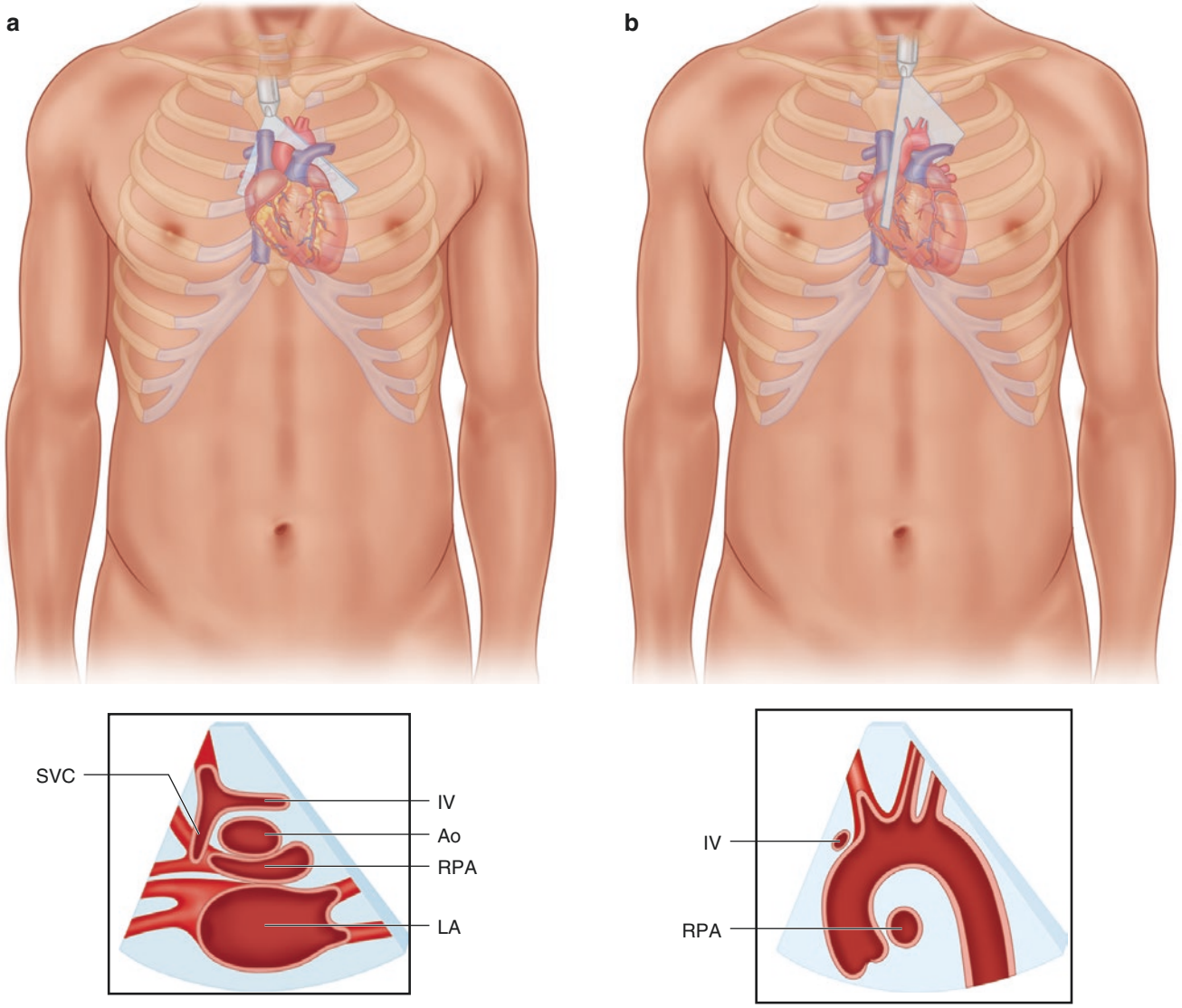

Fig. 1.32 Diagram of the suprasternal short-axis (**a**) and suprasternal long-axis views (**b**). *SVC* superior vena cava, *IV* innominate vein, *AO* aorta, *RPA* right pulmonary artery, *LA* left atrium

range of 0.7–1.1 m/s (Hatle and Angelsen 1985). Antegrade flow in the pulmonary artery during systole is directed away from the transducer (Fig. 1.37). In early diastole there may be a short retrograde flow, which is attributed to backward movement of the blood towards the closed pulmonary valve (Snider et al. 1997). There is only little flow during diastole, although sometimes antegrade flow in late diastole can be noted following right atrial contraction (Grenadier et al. 1984). An increase in systolic antegrade flow velocities in the main pulmonary artery may be due to stenosis of the outflow tract or pulmonary valve or due to an increased flow in the presence of congenital heart disease with left to right shunting. The most likely cause of left to right shunting is atrial septal defect (Chap. 2). Insufficiency of the pulmonary valve results in regurgitant flow directed towards the transducer in diastole (Chap. 7).

1.3.4 Pulmonary Veins

Doppler interrogation of flow in the pulmonary veins can be performed in the apical four-chamber view and in the subcostal coronal view. Visualization of all four pulmonary veins is possible in the suprasternal and high left parasternal short-axis views. In the latter plane, however, the angle of Doppler interrogation may be less favourable than in the previous views, resulting in some underestimation of the flow velocities. In order to measure flow within the veins, the sample volume should be

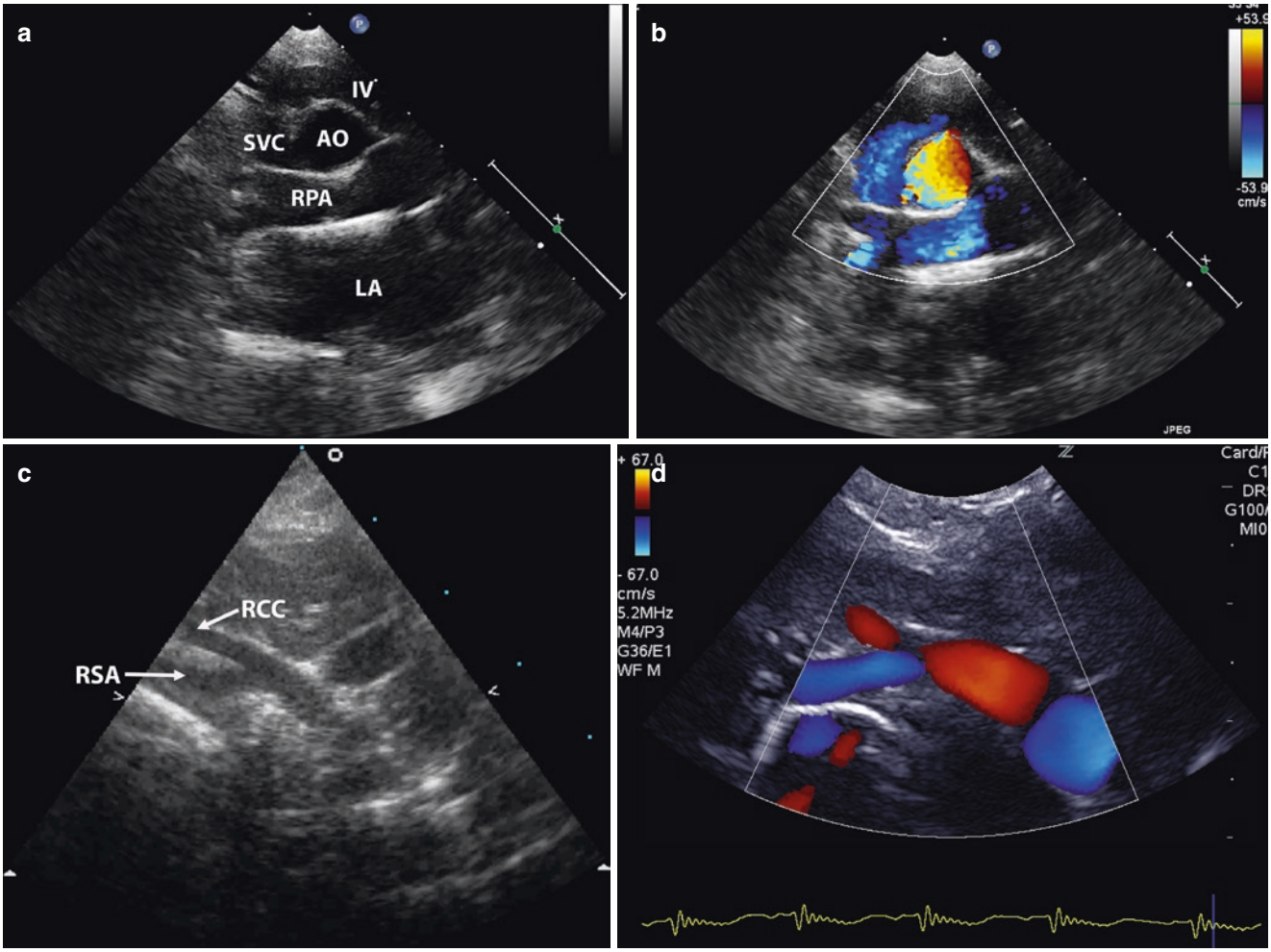

Fig. 1.33 Suprasternal short axis displaying the innominate vein (*IV*) connecting to the superior vena cava (*SVC*) and the aorta (*AO*) in cross section (**a**). The right pulmonary artery (*RPA*) and left atrium (*LA*) are displayed below the aorta. Colour Doppler shows flow in the RPA up to the hilum (**b**). Cranial tilt and clockwise rotation of the transducer result in this longitudinal view of the innominate artery (**c**) and its bifurcation into the right common carotid (*RCC*) and subclavian artery (*RSA*) which is confirmed by colour Doppler (**d**)

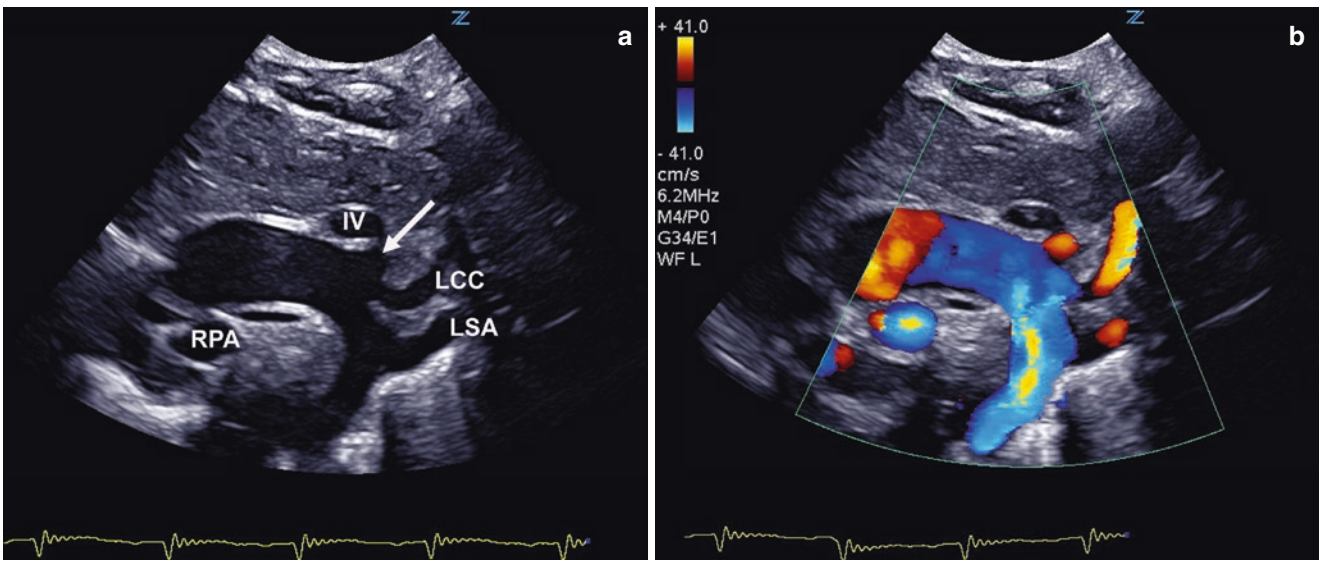

Fig. 1.34 Suprasternal long-axis view of the aortic arch (**a**), depicting innominate artery (*arrow*), left common carotid (*LCA*) and left subclavian artery (*LSA*); the right pulmonary artery is displayed underneath (*RPA*) the innominate vein (*IV*) above the aorta. Colour Doppler showing systolic flow in the aorta and brachiocephalic arteries (**b**)

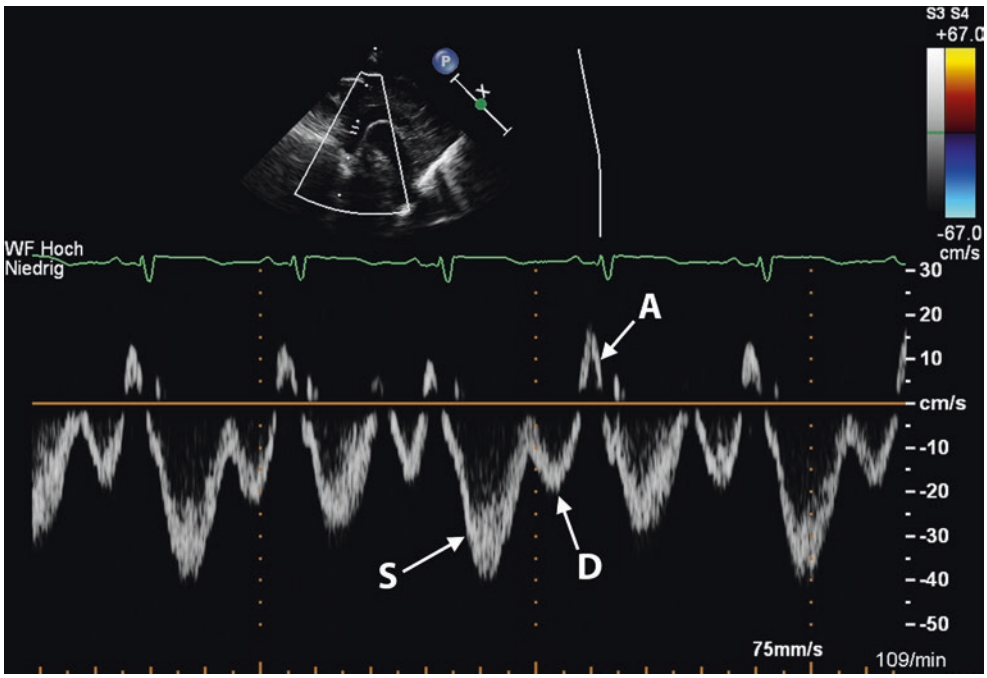

Fig. 1.35 Pulsed wave Doppler interrogation in the superior vena cava from a suprasternal window shows flow directed towards the right atrium during systole (*S wave*) and during diastole (*D wave*). There is a short period of reverse flow during atrial contraction (*A wave*)

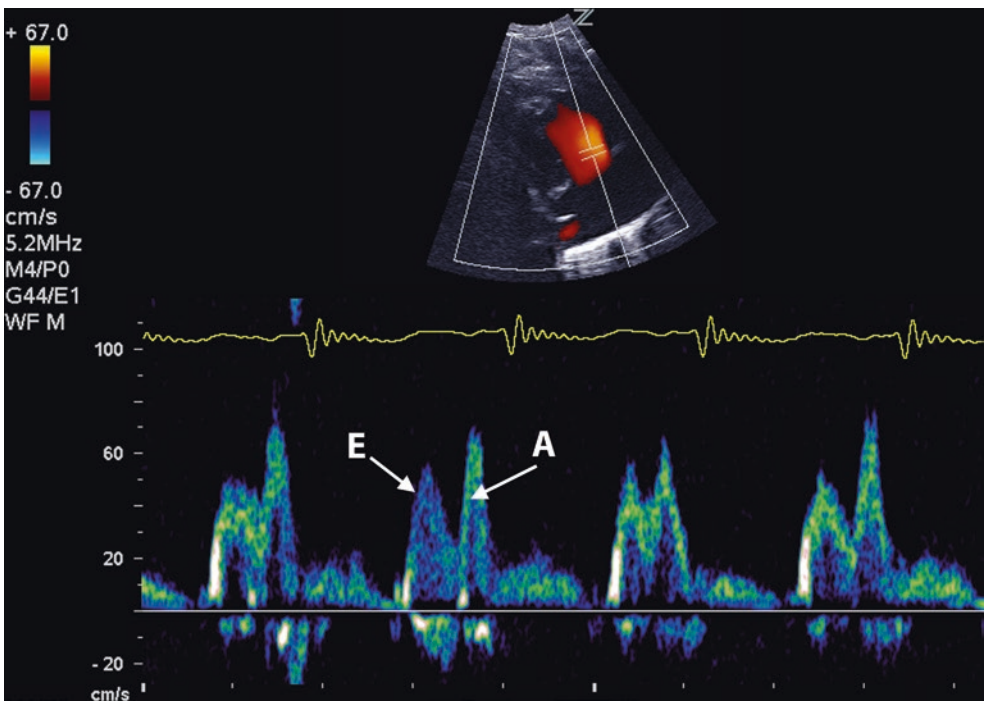

Fig. 1.36 Pulsed wave Doppler recording of tricuspid valve inflow in the parasternal long axis shows diastolic forward flow during rapid ventricular filling (*E wave*) and during atrial systole (*A wave*). In this normal neonate, the *A wave* exceeds the *E wave*

placed proximal to its connection with the left atrium (Snider et al. 1997). Normal pulmonary venous flow is characterized by a triphasic flow pattern (Fig. 1.38). Forward flow in systole results in the S wave (Mertens et al. 2010; Snider et al. 1997). The S wave may exhibit a biphasic peak, representing forward flow during atrial relaxation and ventricular suction effect due to downward movement of the mitral annulus during ventricular contraction (Klein and Tajik 1991;Nishimura et al. 1990). Diastolic antegrade flow, represented by the D wave, corresponds with opening of the mitral valve, decrease of atrial pressure and rapid ventricular filling (Mertens et al. 2010; Snider et al. 1997). Atrial contraction may result in a short reverse flow in the pulmonary veins termed A wave (Fig. 1.38). While normal flow velocities of S and D waves are similar in childhood in

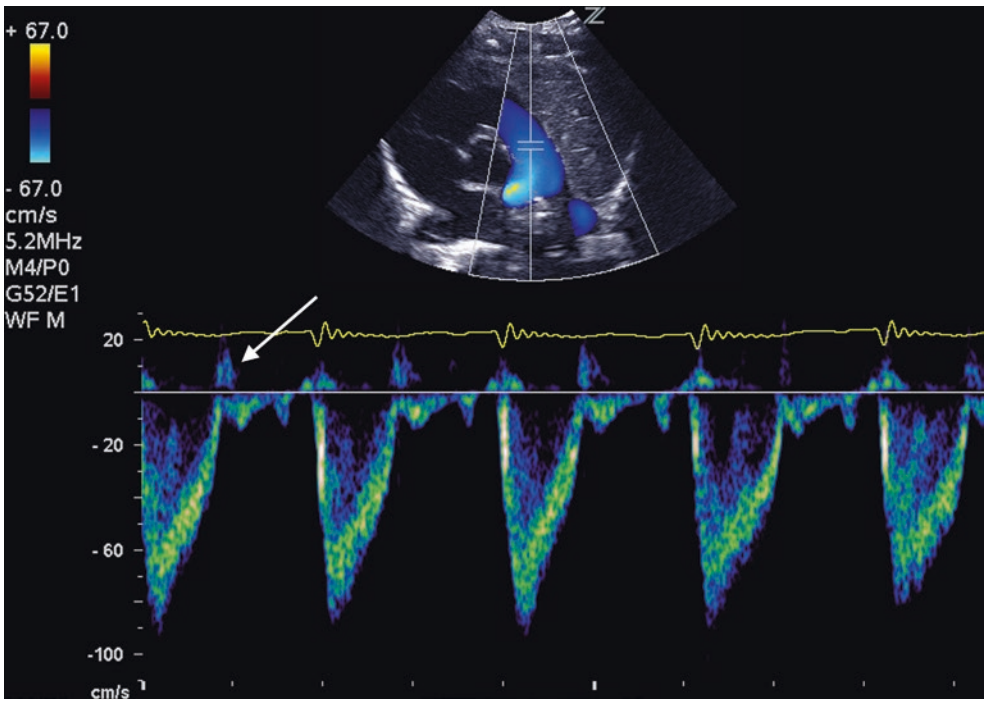

Fig. 1.37 Pulsed wave Doppler recording of flow in the main pulmonary artery, recorded in the parasternal short axis view showing antegrade systolic flow followed by minimal retrograde flow in early diastole (*arrow*)

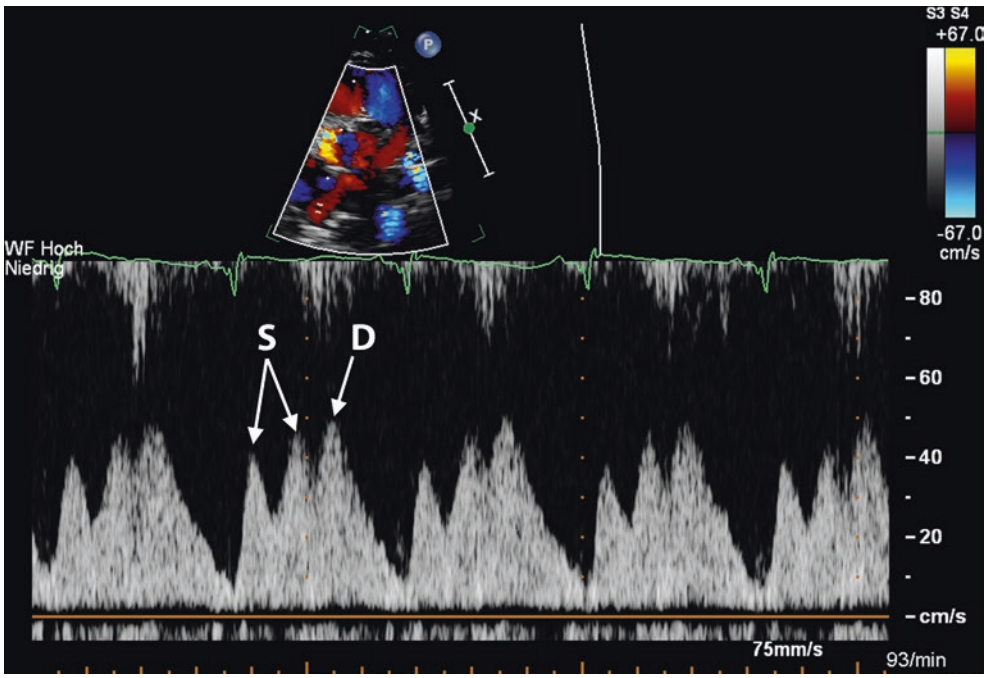

Fig. 1.38 Pulsed wave Doppler interrogation of the pulmonary veins in a high parasternal short axis showing a triphasic pattern with systolic antegrade flow (*S* wave in this patient exhibiting a biphasic peak), diastolic antegrade flow (*D* wave) and minimal retrograde flow following atrial contraction (*arrow*)

the range of 50 cm/s, in adulthood, flow during systole becomes more prominent with increasing age (Klein and Tajik 1991; Snider et al. 1997).

Forward flow in the pulmonary veins is influenced by many factors including left ventricular systolic and diastolic function (Mertens et al. 2010; Snider et al. 1997). Pulmonary venous flow velocities are less influenced by respirations than systemic venous flow. Similar to flow patterns in systemic veins, sinus tachycardia may result in fusion of S and D waves (Snider et al. 1997).

1.3.5 Mitral Valve

The best plane for recording flow across the mitral valve is the apical four-chamber view. The highest velocities of

diastolic inflow into the left ventricle are recorded with the sample volume placed at the tip of the mitral valve leaflets. Similar to the tricuspid valve, diastolic mitral valve inflow exhibits a biphasic flow pattern (Fig. 1.39). The E wave represents rapid left ventricular filling following diastolic opening of the mitral valve. The A wave represents diastolic inflow following atrial contraction. In analogy to the tricuspid valve, the ratio of E to A wave velocities is subject to significant change in early infancy. While the peak velocity of the A wave exceeds the E wave in the fetus and in the neonatal period, the peak velocity of the E wave is higher as compared to the A wave in infants and children resulting in an E/A velocity ratio of 1,9 + 0.4 (Riggs et al. 1989; Snider et al. 1985). The inverted E/A velocity ratio in the fetus and neonate is attributed to decreased compliance of the ventricles possibly related to immaturity of the myocardium resulting in increased dependency on diastolic filling by atrial contraction (Mertens et al. 2010; Snider et al. 1997).

1.3.6 Left Ventricular Outflow Tract and Aorta

Flow velocities in the left ventricular outflow tract are best recorded in the apical five-chamber view with anterior tilt of the transducer displaying the ascending aorta (Fig. 1.40). Normal peak velocities in children are 1 m/s with a range of 0.7–1.2 m/s (Davidson et al. 1991; Hatle and Angelsen 1985). Flow in the ascending aorta can be recorded again from the five-chamber view, from a high right parasternal position or from the suprasternal notch (Figs. 1.40 and 1.41). In patients with valvular aortic stenosis, it is not uncommon that flow across the aortic valve is eccentric and directed towards the lateral wall of the ascending aorta. In this situation, it is frequently the high right parasternal position, which allows a better alignment of the Doppler beam with the jet across the valve. Normal systolic flow in the ascending aorta has a more rapid rate of acceleration as compared to flow in the pulmonary artery. In early diastole, there is a small

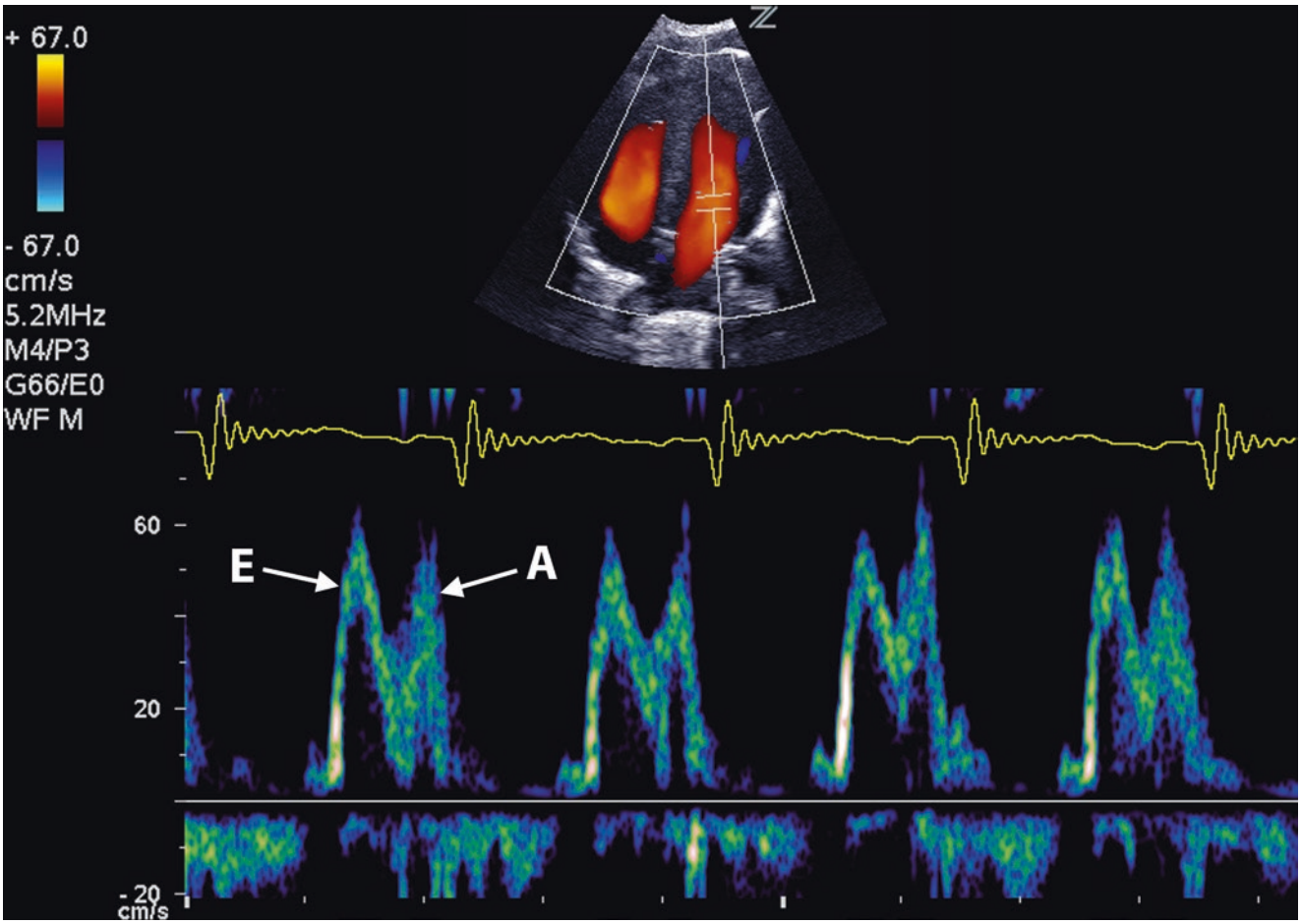

Fig. 1.39 Pulsed wave Doppler recording of mitral valve inflow in the apical four-chamber view in a normal neonate diastolic forward flow occurring with rapid ventricular filling (*E wave*) and flow during atrial systole (*A wave*). In this 4-week-old neonate, E and A wave velocities are almost equal, while E wave velocities are higher than A wave velocities in older children

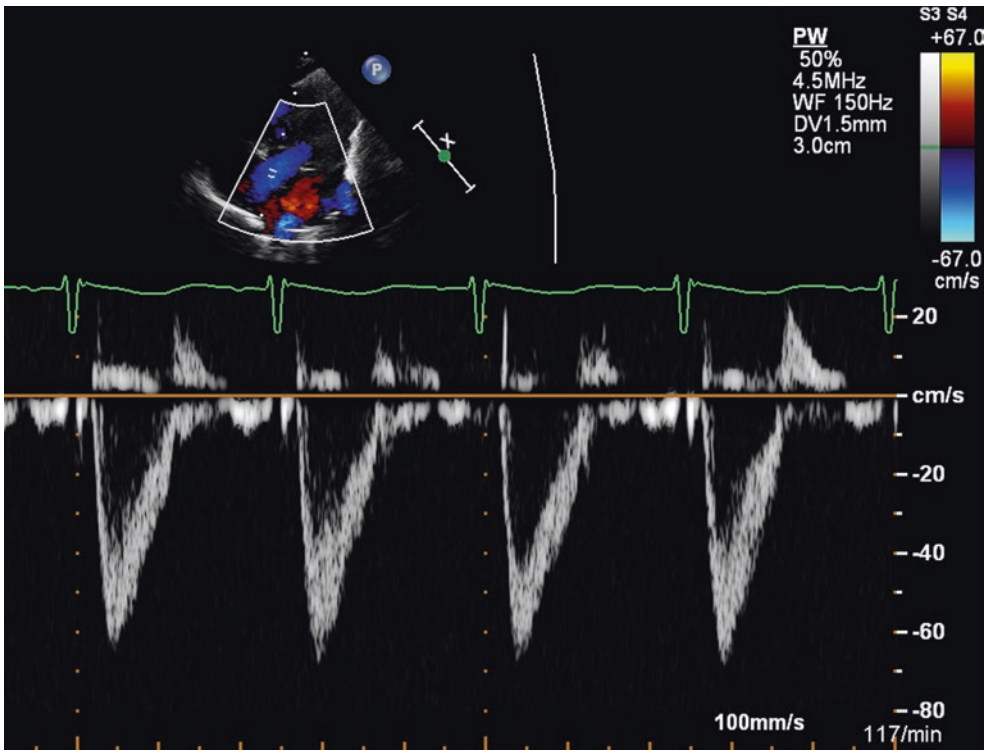

Fig. 1.40 Pulsed wave Doppler interrogation of the left ventricular outflow tract in the apical five-chamber view shows antegrade flow during systole, followed by minimal retrograde flow in early diastole and minimal antegrade flow during diastole

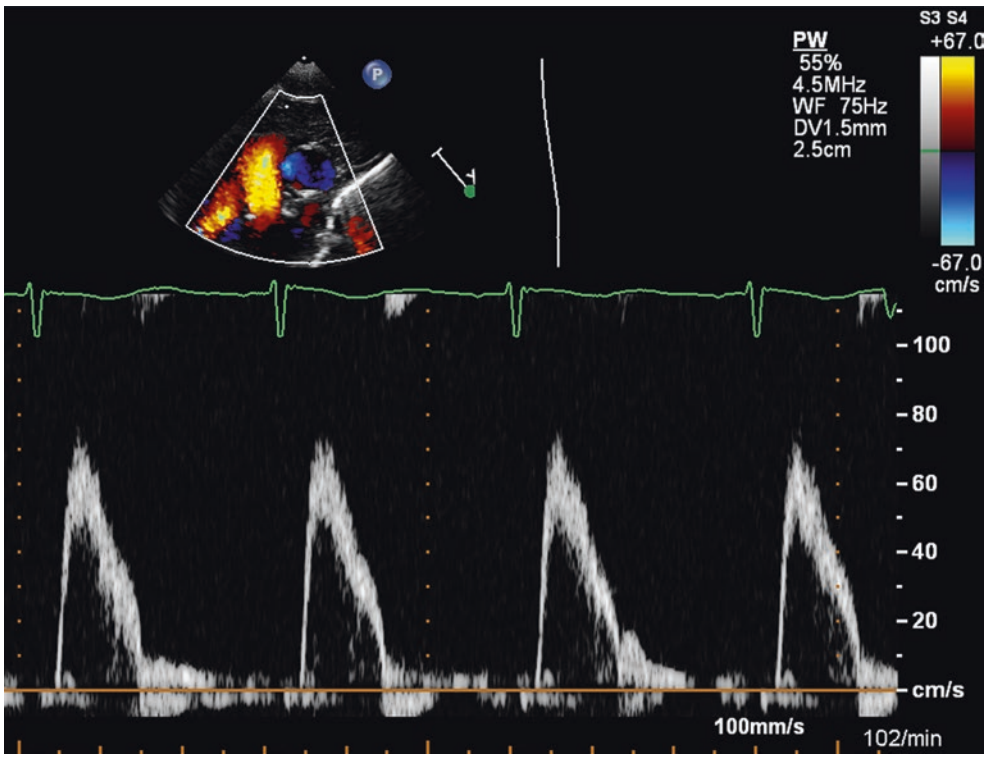

Fig. 1.41 Pulsed wave Doppler interrogation of the ascending aorta in the right parasternal view shows systolic flow directed towards the transducer

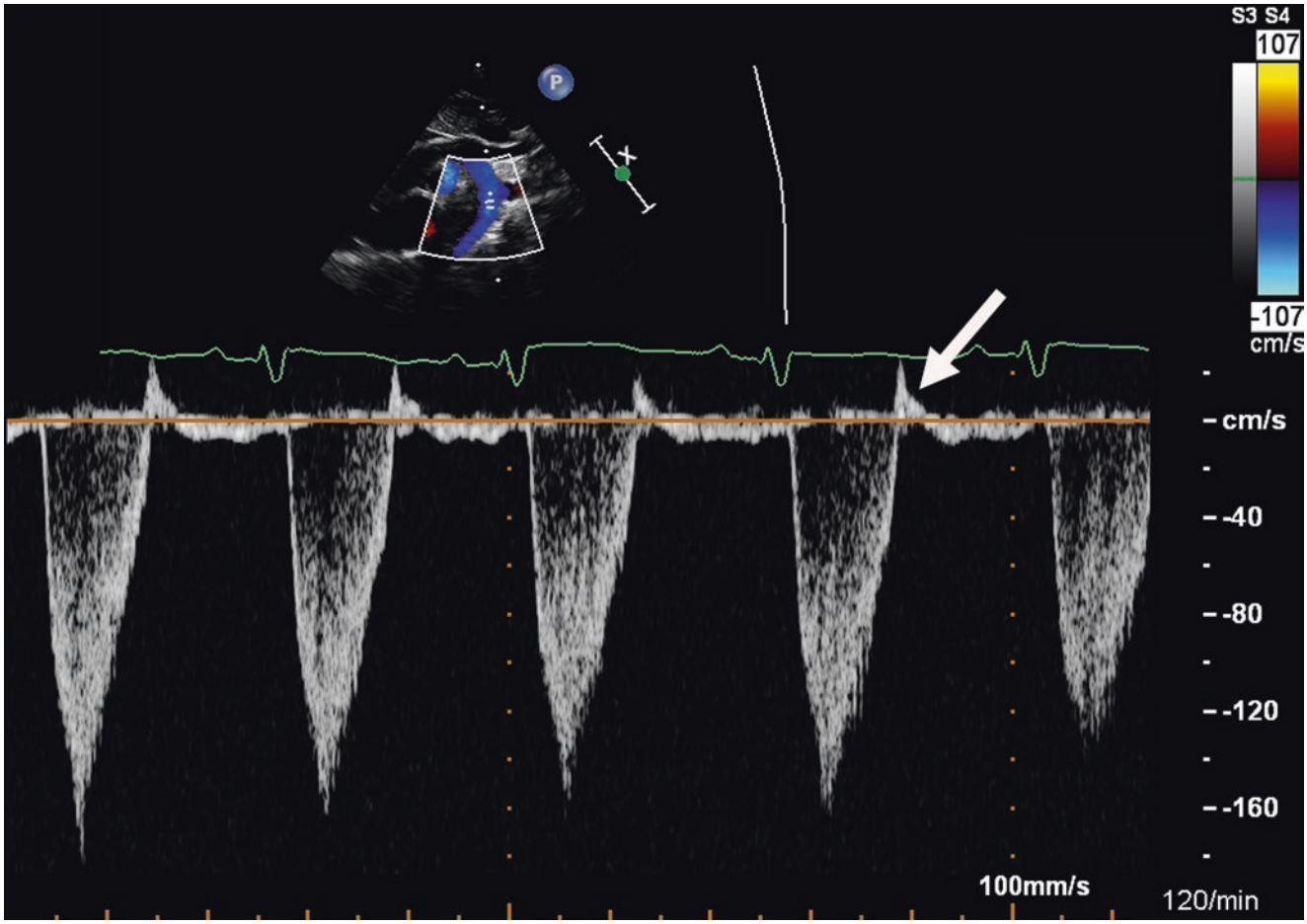

Fig. 1.42 In the suprasternal long axis view, pulsed wave Doppler of the descending aorta shows systolic flow directed away from the transducer, followed by minimal retrograde flow in early diastole (*arrow*) and low velocity antegrade flow in late diastole

amount of retrograde flow due to backward blood flow towards the closed aortic valve (Fig. 1.41). Maximal systolic flow velocity in children has been reported to be 1.5 m/s with a range of 1.2–1.8 m/s (Hatle and Angelsen 1985). Flow velocities appear to remain relatively constant during childhood independent of age (Grenadier et al. 1984; Seear et al. 1991). Flow in the descending aorta is best recorded from the suprasternal notch (Fig. 1.42). Normal flow velocities have been reported with 0.88 m/s and a range of 0.51–0.88 (Grenadier et al. 1984).

1.4 Doppler Echocardiography in the Assessment of Haemodynamics

Doppler echocardiography has become a valuable tool in the haemodynamic assessment of cardiac function. To a large extent, haemodynamic evaluation is based on the determination of pressure gradients. Doppler-derived determination of pressure gradients is based on the Bernoulli equation, which describes the relation of pressure and flow velocity in a system of steady, incompressible and frictionless flow (DeGroff et al. 2002; Mertens et al. 2010). Since viscous forces and local acceleration can be neglected in the clinical setting, it is possible to use the modified Bernoulli equation (DeGroff et al.2002).

$$\text{Pressure gradient}\left(\text{mmHg}\right) = \tfrac{1}{2}\rho\left(V_2^2 - V_1^2\right)$$

V_2 represents the velocity distal and V_1 the velocity proximal to the obstruction given in m/s and ρ represents the density of blood. Since the term ½ ρ for blood is approximately equal to 4 and since in many clinical settings, the velocity proximal to the stenosis is < 1.5 m/s, the equation can be simplified even further by omitting V_1 (DeGroff et al. 2002; Feigenbaum et al. 2005).

$$\text{Pressure gradient}\left(\text{mmHg}\right) = 4\left(V_2^2\right)$$

This simplified Bernoulli equation has been integrated in the software of echo machines. It can be employed to obtain a number of important haemodynamic informations. These include calculation of peak instantaneous gradients across the right and left ventricular outflow tracts and their valves, as well as calculation of gradients across the aortic isthmus, ductus arteriosus and ventricular septal defects. Furthermore it can be employed to estimate noninvasively the right ventricular and pulmonary arterial pressure. It has to be kept in mind, however, that application of the simplified Bernoulli equation is associated with certain limitations, which have to be included in the interpretations of its results.

1.5 Calculation of Gradients Across the Outflow Tracts and Aortic and Pulmonary Valve

Obstruction of the outflow tract or semilunar valves results in turbulence and acceleration of blood flow. Since flow velocity across the obstruction correlates with the severity of the stenosis, the pressure gradient can be calculated with the simplified Bernoulli equation based on the maximal velocity across the obstruction. In the presence of significant obstruction, maximal flow velocities in the right or left ventricular outflow tract usually exceed the range of 2.5–3 m/s and therefore the spectrum of velocities that can be depicted by pulsed wave Doppler. Possible measures to increase the velocity range that can be depicted by pulsed wave Doppler include optimization of the frequency scale including use of the HPRF mode, shifting of the baseline and change of the transducer to a lower frequency probe. Otherwise determination of maximal blood flow velocity requires the application of continuous wave Doppler.

Determination of the gradient across the outflow tracts based on Doppler measurement of peak flow velocity delivers the so-called peak instantaneous gradient. The peak instantaneous gradient refers to the maximal difference between ventricular and arterial pressures that occurs at any time during cardiac systole (Fig. 1.43). On the contrary during cardiac catheterization, it is usually the peak-to-peak gradient that is recorded, representing the difference between the peak systolic pressure in the ventricle and in the respective artery (Fig. 1.43). Many studies in the literature dealing with natural history, treatment and long-term outcome of congenital heart disease are based on catheter-derived peak-to-peak gradients. These are lower than peak instantaneous gradients. Since both gradients describe the pressure gradient between the ventricle and artery at different time points during the cardiac cycle, it is not correct however to conclude that Doppler measurements overestimate the severity of the obstruction.

Doppler-derived determination of the outflow tract gradient has several shortcomings that have to be included in the interpretation of the results (Mertens et al. 2010).

1. The major pitfall results from underestimation of the maximal velocity due to suboptimal alignment of the Doppler beam with the jet across the stenosis. This applies especially for valvular stenoses with eccentric jets. While an angle of up to 15° between the Doppler beam and the jet can be tolerated, angles > 15° result in a significant decrease of the Doppler shift and a significant underestimation of the maximal velocity. To ensure that the maximal gradient has been recorded, it is necessary to perform Doppler interrogation of the flow

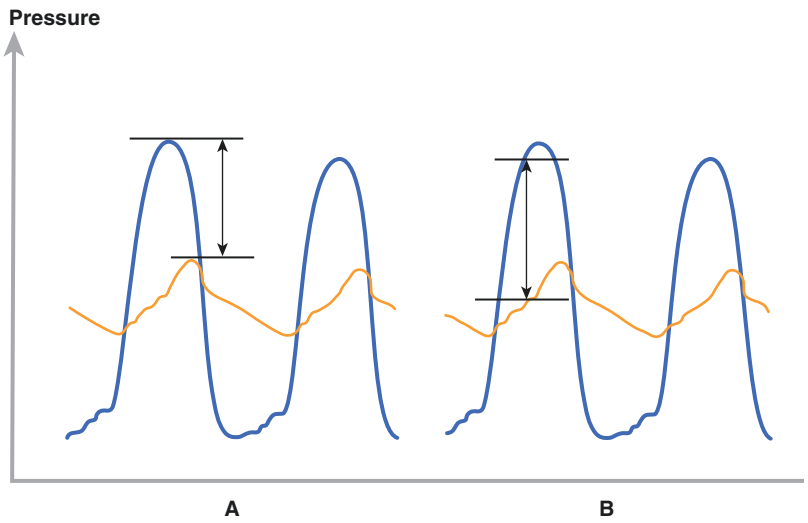

Fig. 1.43 Diagram showing the difference between peak-to-peak and peak instantaneous gradients in the setting of aortic stenosis with simultaneous pressure tracings of the left ventricle (blue tracing) and aorta (red tracing). The peak-to-peak gradient (*A*) represents the difference of peak systolic pressures in the left ventricle and aorta, while the peak instantaneous gradient (*B*) refers to the maximal pressure difference occurring during ventricular systole

velocity across the obstruction in different planes. For example, in the presence of left ventricular outflow tract obstruction, Doppler interrogation should be performed in the apical five-chamber view, the high right parasternal view, the suprasternal notch and from the subcostal window. Calculation of the gradient should be based on the maximal velocity recorded in the different views.

2. In neonates with critical stenoses, the ventricle may develop myocardial failure and become unable to create adequate flow across the stenosis. In the context of low cardiac output, the gradient across the outflow tract no longer correlates with the severity of the obstruction and may be inadequately low. Especially in neonates with critical left ventricular outflow tract obstruction, the gradient should always be interpreted in the context of the morphology of the outflow tract obstruction and the systolic function of the left ventricle (DeGroff et al. 2002).
3. The simplified Bernoulli equation neglects V_1, the velocity proximal to the stenosis. This simplification is acceptable as long as the velocity proximal to the stenosis does not exceed velocities of 1 m/s. In the presence of an increased proximal velocity, the simplified equation may result however in overestimation of the gradient. An increased proximal velocity may be encountered either in patients with obstruction at more than one level (e.g. in the presence of subvalvular and valvular stenosis) and in the presence of an increased volume passing the interrogated vascular segment. The latter situation is encountered in patients with intracardiac shunt (e.g. atrial septal defects in combination with pulmonary stenosis) or in valvular lesions combining stenosis and regurgitation. In these situations, the modified Bernoulli equation should be applied, which includes measurement of the proximal velocity (Feigenbaum et al. 2005; Snider et al. 1997).

$$\text{Pressure gradient}\left(\text{mmHg}\right) = 4\left(v_2^{\,2} - v_1^{\,2}\right)$$

4. Application of the simplified Bernoulli equation is problematic in the evaluation of flow in small vessels with long-segment tubular stenoses since the equation does not measure losses due to viscous forces (DeGroff et al. 2002; Mertens et al. 2010).
5. In the presence of high velocity jets, a phenomenon, which is termed pressure recovery, may result in overestimation of the peak velocity measured by Doppler interrogation. Within a tight stenosis, some part of the energy is converted into kinetic energy and reconverted distal to the obstruction back into potential energy (DeGroff et al. 2002; Mertens et al. 2010). This process of pressure recovery is not included in Doppler measurements and may result in overestimation of peak velocity and calculated peak instantaneous gradients especially in tubular stenoses (Akgun et al. 2014; Bahlmann et al. 2010; Villavicencio et al. 2003; Yoganathan et al. 1987).

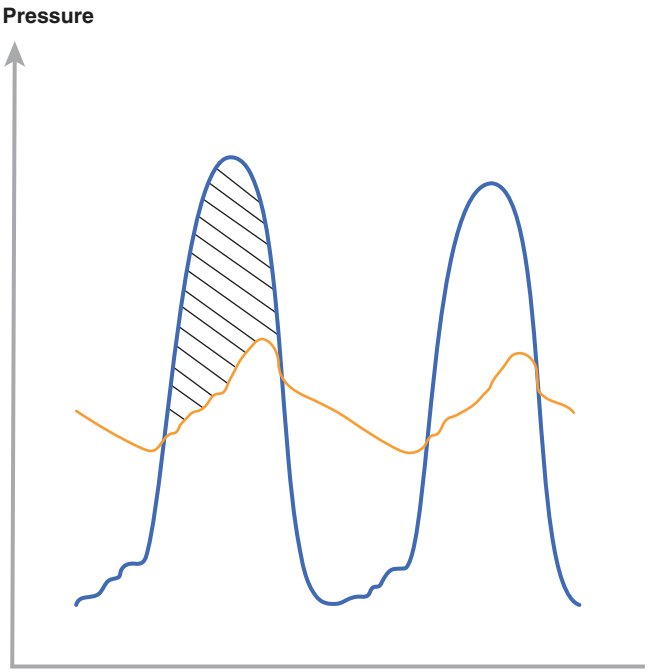

Fig. 1.44 Diagram showing the mean gradient in the setting of aortic valve stenosis with simultaneous pressure tracings of the left ventricle and aorta. The mean gradient represents the average of peak instantaneous gradients obtained during systole

Valuable additional information in the assessment of valvular stenoses and outflow tract obstructions is provided by calculation of the mean gradient (Fig. 1.44). It is obtained by tracing of the Doppler flow curve across the obstruction followed by electronic calculation of the average of peak instantaneous gradients (DeGroff et al. 2002; Mertens et al. 2010). The resulting mean gradient is significantly lower than the peak instantaneous gradient. Especially in the assessment of aortic stenosis, it correlates better with invasive gradients of cardiac catheterization, and therefore calculation of the mean gradient has become integral part of the routine assessment of outflow tract obstructions and stenoses of the atrioventricular valves.

1.6 Determination of Right Ventricular and Pulmonary Arterial Pressure

Noninvasive calculation of right ventricular and pulmonary arterial pressure provides important information not only in patients with congenital heart disease but also in premature infants and neonates and infants requiring intensive care treatment for other reasons. Noninvasive Doppler assessment of right ventricular or pulmonary artery pressure based on the simplified Bernoulli equation is possible under one of the following preconditions:

- Tricuspid regurgitation (Skinner et al. 1991, 1996)
- Pulmonary regurgitation (Mertens et al. 2010)
- Presence of a ventricular septal defect (Marx et al. 1985; Murphy et al. 1986)
- Patency of the ductus arteriosus (Musewe et al. 1990; Musewe 1987)

Even in patients without pathology of the tricuspid valve, it may be possible to obtain a pulsed wave or continuous wave Doppler tracing of tricuspid regurgitation (Choong et al. 1989;Lee and Lin 2010;Skinner et al. 1991, 1996). The systolic pressure in the right ventricle can be estimated based on the peak velocity of the regurgitant jet according to the following equation (Fig. 1.45):

$$\text{Systolic pressure RV} = \text{Gradient tricuspid regurgitation} + \text{Mean right atrial pressure}$$

In patients with a central venous line, the mean central venous pressure can be added in the equation; otherwise, it can be estimated with 5–10 mmHg (Mertens et al. 2010). In the absence of obstruction of the right ventricular outflow tract and the pulmonary valve, the systolic pressure in the right ventricle will be equal to the pulmonary artery systolic pressure.

Doppler interrogation of minor pulmonary regurgitation is frequently possible in children even in the presence of a normal pulmonary valve. Doppler tracing of pulmonary regurgitation reveals a peak diastolic and an end-diastolic velocity. In children the gradient calculated based on the peak diastolic velocity correlates well with the mean pulmonary artery pressure (Mertens et al. 2010). The gradient calculated based on the end-diastolic velocity correlates with pulmonary arterial diastolic pressure. An estimated mean right atrial pressure is added in both calculations.

In patients with pathologic shunts at the level of the ventricles or great arteries, the pressure gradient between both ventricles or arteries can be used to determine the systolic pressure in the right ventricle and in the pulmonary artery.

In the presence of a ventricular septal defect, the pressure difference between both ventricles can be calculated with the simplified Bernoulli equation based on the maximal flow velocity across the defect (gradient VSD = $4v^2$). *If the defect is large and results in equal pressure of both ventricles*, *flow velocities over the defect will be low*, *indicating absence of a gradient between both ventricles*. If the defect is small with preservation of low pressure in the right ventricle, Doppler interrogation of flow across the

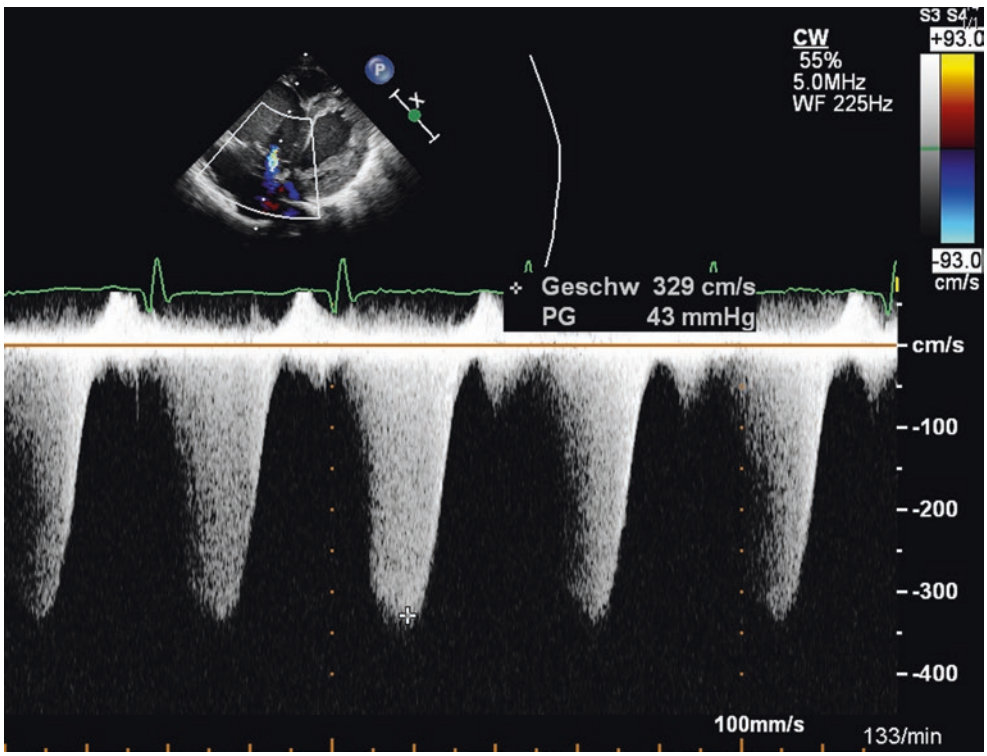

Fig. 1.45 Continuous wave Doppler recording of tricuspid regurgitation in a patient with elevated pulmonary artery pressure. According to a maximal systolic regurgitation velocity of 329 cm/s from the right ventricle to right atrium, the simplified Bernoulli equation calculates a gradient of 43 mmHg. Assuming a mean pressure of 10 mmHg in the right atrium, right ventricular systolic pressure can be estimated with 53 mmHg. In the absence of pulmonary stenosis, this would be identical to systolic pulmonary artery pressure

VSD reveals high flow velocities according to the significant pressure gradient between both ventricles.

Based on the gradient across the VSD, it is possible to estimate the systolic RV pressure (Marx et al. 1985;Murphy et al. 1986): in the absence of obstruction of the left ventricular outflow tract, the systolic blood pressure (which can be measured noninvasively) equals the systolic pressure in the left ventricle. The systolic right ventricular pressure can be obtained by subtraction of the gradient across the ventricular septal defect from the systolic left ventricular pressure.

$$\text{Systolic pressure RV} - \underset{\text{Gradient across VSD}}{\text{Systolic blood pressure}}$$

In the absence of an obstruction of the right ventricular outflow tract or the pulmonary valve, the systolic right ventricular pressure will be identical to the systolic pulmonary artery pressure.

Since the ductus arteriosus represents a communication between systemic and the pulmonary circulation, flow velocities across the ductus can be used to estimate pressure differences between both circulations (Musewe et al. 1990; Musewe et al. 1987). According to the simplified Bernoulli equation, the maximal flow velocity across the ductus allows calculation of the systolic pressure difference between systemic and pulmonary circulation. Following oscillometric measurement of the patient's blood pressure, the pulmonary artery pressure can be calculated noninvasively.

$$\text{Systolic blood pressure} - \text{Gradient across the ductus arteriosus} = \text{Systolic pulmonary arterial pressure}$$

Large ducts, with significant elevation of the pulmonary artery pressure, result in low-pressure gradients between both circulations. On the other hand, small ducts, associated with normal pulmonary arterial pressures, will present with high flow velocities exceeding 4 m/s. It has to be kept in mind, however, that elevation of pressure artery pressure for other reasons (e.g. physiologically elevated pulmonary vascular resistance in the neonatal period) also results in low gradients across the ductus arteriosus independent of its size.

Important preconditions for all these methods of noninvasive determination of pulmonary arterial pressures are:

- Exact alignment of the Doppler beam with the interrogated regurgitant jet or shunt flow to avoid underestimation of the velocity.
- Evaluation should be performed only if it is possible to obtain a clear Doppler signal.
- Care should be taken not to miss other pathologies like right or left ventricular outflow tract obstruction.
- Noninvasive determination of blood pressure should be performed simultaneously under identical haemodynamic conditions.

1.7 Noninvasive Determination of Stroke Volume and Cardiac Output

Since flow across a valve or inside a vessel can be described as the product of flow velocity and cross-sectional area (CSA) of the respective vessel, noninvasive determination of flow can be achieved based on measurement of these parameters (Oh et al. 2007). Since flow velocities are variable in the cardiovascular system, flow during a certain time period is integrated by tracing of the Doppler flow curve and calculation of the time velocity integral (TVI). The cross-sectional area of the respective vessel is calculated based on its diameter (D) with the assumption that the latter is circular: $(D/2)^2 \times \pi$. Stroke volume (SV) is calculated according to

$$SV = CSA \times TVI$$

Usually cardiac output measurements are performed in the right and left ventricular outflow tract. Theoretically simultaneous measurements of pulmonary and systemic stroke volume could be used to determine the magnitude of cardiac shunting, e.g. in the presence of an atrial septal defect (Oh et al. 2007). This technique however has severe limitations. The most significant source of error is due to inaccurate determination of the cross-sectional area of the vessel (Snider et al. 1997). Therefore noninvasive determination of stroke volume presently plays no significant role in the clinical assessment in paediatric cardiology.

1.8 Calculation of Valve Area

The continuity equation can be employed to estimate the unknown area of a valve (Mertens et al. 2010;Oh et al. 2007). This equation is based on the fact that the flow rate remains constant in a closed vascular system. The product of CSA and flow at a proximal point should be identical to that one at a more distal point.

$$CSA_1 \times TVI_1 = CSA_2 \times TVI_2$$

If it is possible to measure the flow at two different locations in a continuous vascular system and if the cross-sectional area is known at one of these locations, it is possible to calculate the cross-sectional area at the second location.

$$CSA_2 = CSA_1 \times TVI_1 / TVI_2$$

Calculation of the aortic valve area requires calculation of the time velocity integral by Doppler interrogation in the apical five-chamber view and measurement of the diameter of the left ventricular outflow tract for calculation of CSA1. Finally flow across the stenotic valve representing TVI_2 is determined (e.g. from a right parasternal view) (see also Fig. 19.14).

The advantage of this method is that it is independent of flow across the stenotic vessel. For example, in the presence of low cardiac output due to severe myocardial failure in aortic stenosis, the pressure gradient may be low and may not reflect the true severity of the stenosis. Calculation of the aortic valve area is dependent however on exact determination of flow (TVI_1 and TVI_2) and on exact measurement of CSA_1. Due to these limitations and since cardiac failure in the context of valvular heart disease is rare in children beyond the neonatal period, clinical decisions in paediatric valvular heart disease are usually made based on pressure gradients (Lai and Ko 2009; Mertens et al. 2010).

References

Akgun T, Karabay CY et al (2014) Discrepancies between Doppler and catheter gradients in ventricular septal defect: a correction of localized gradients from pressure recovery phenomenon. Int J Cardiovasc Imaging 30(1):39–45

Bahlmann E, Cramariuc D et al (2010) Impact of pressure recovery on echocardiographic assessment of asymptomatic aortic stenosis: a SEAS substudy. JACC Cardiovasc Imaging 3(6):555–562

Choong CY, Abascal VM et al (1989) Prevalence of valvular regurgitation by Doppler echocardiography in patients with structurally normal hearts by two-dimensional echocardiography. Am Heart J 117(3):636–642

Daubeney PE, Blackstone EH et al (1999) Relationship of the dimension of cardiac structures to body size: an echocardiographic study in normal infants and children. Cardiol Young 9(4):402–410

Davidson WR Jr, Pasquale MJ et al (1991) A Doppler echocardiographic examination of the normal aortic valve and left ventricular outflow tract. Am J Cardiol 67(6):547–549

DeGroff CG (2002) Doppler echocardiography. Pediatr Cardiol 23(3):307–333

Feigenbaum H, Armstrong WF et al (2005) Feigenbaum's echocardiography. Lippincott Williams & Wilkins, Philadelphia/Baltimore/New York/London

Grenadier E, Oliveira Lima C et al (1984) Normal intracardiac and great vessel Doppler flow velocities in infants and children. J Am Coll Cardiol 4(2):343–350

Hatle L, Angelsen B (1985) Doppler ultrasound in cardiology: physical principles and clinical applications. Lea & Febiger, Philadelphia

Higgins CB, Silverman NH et al (1990) Congenital heart disease. Echocardiography and magnetic resonance imaging. Raven, New York

Klein AL, Tajik AJ (1991) Doppler assessment of pulmonary venous flow in healthy subjects and in patients with heart disease. J Am Soc Echocardiogr 4(4):379–392

Lai WW, Geva T et al (2006) Guidelines and standards for performance of a pediatric echocardiogram: a report from the Task Force of the Pediatric Council of the American Society of Echocardiography. J Am Soc Echocardiogr Off Publ Am Soc Echocardiogr 19(12):1413–1430

Lai WW, Ko HH (2009) The normal pediatric echocardiogram. In: Lai WW, Mertens LL, Cohen MS, Geva T (eds) Echocardiography in pediatric and congenital heart disease. Blackwell Publishing Ltd, Chichester

Lai WW, Mertens LL et al (2009) Echocardiography in pediatric and congenital heart disease. Blackwell Publishing Ltd, Chichester, UK

Lee ST, Lin MH (2010) Color Doppler echocardiographic assessment of valvular regurgitation in normal infants. J Formos Med Assoc 109(1):56–61

Marx GR, Allen HD et al (1985) Doppler echocardiographic estimation of systolic pulmonary artery pressure in pediatric patients with interventricular communications. J Am Coll Cardiol 6(5):1132–1137

Mertens LL, Rigby ML et al (2010) Cross sectional echocardiographic and Doppler imaging. In: Anderson RH, Baker EJ, Penny DJ et al (eds) Pediatric cardiology. Churchill Livingstone/Elsevier, Philadelphia

Meyer RJ, Goldberg SJ et al (1993) Superior vena cava and hepatic vein velocity patterns in normal children. Am J Cardiol 72(2):238–240

Murdison KA (1996) Ultrasonic imaging of vascular rings and other anomalies causing tracheobronchial compression. Echocardiography 13(3):337–356

Murphy DJ Jr, Ludomirsky A et al (1986) Continuous-wave Doppler in children with ventricular septal defect: noninvasive estimation of interventricular pressure gradient. Am J Cardiol 57(6):428–432

Musewe NN, Smallhorn JF et al (1987) Validation of Doppler-derived pulmonary arterial pressure in patients with ductus arteriosus under different hemodynamic states. Circulation 76(5):1081–1091

Musewe NN, Poppe D, Smallhorn JF, Hellman J, Whyte H, Smith B, Freedom RM (1990) Doppler echocardiographic measurement of pulmonary artery pressure from ductal Doppler velocities in the newborn. J Am Coll Cardiol 15(2):446–456

Nishimura RA, Abel MD et al (1990) Relation of pulmonary vein to mitral flow velocities by transesophageal Doppler echocardiography. Effect of different loading conditions. Circulation 81(5):1488–1497

Oh JK, Seward JB et al (2007) The echo manual. Baltimore, New York, London, Lippincott Williams & Wilkins, Philadelphia

Reynolds T, Appleton CP (1991) Doppler flow velocity patterns of the superior vena cava, inferior vena cava, hepatic vein, coronary sinus, and atrial septal defect: a guide for the echocardiographer. J Am Soc Echocardiogr 4(5):503–512

Riggs TW, Rodriguez R et al (1989) Doppler echocardiographic evaluation of right and left ventricular diastolic function in normal neonates. J Am Coll Cardiol 13(3):700–705

Seear MD, D'Orsogna L et al (1991) Doppler-derived mean aortic flow velocity in children: an alternative to cardiac index. Pediatr Cardiol 12(4):197–200

Skinner J, Alverson D et al (2000) Echocardiography for the neonatologist. Churchill Livingstone, Edinburgh, London, New York

Skinner JR, Boys RJ et al (1996) Estimation of pulmonary arterial pressure in the newborn: study of the repeatability of four Doppler echocardiographic techniques. Pediatr Cardiol 17(6):360–369

Skinner JR, Boys RJ et al (1991) Non-invasive assessment of pulmonary arterial pressure in healthy neonates. Arch Dis Child 66(4 Spec No):386–90

Snider AR, Gidding SS et al (1985) Doppler evaluation of left ventricular diastolic filling in children with systemic hypertension. Am J Cardiol 56(15):921–926

Snider RA (1996) Congenital anomalies of the aortic arch. Echocardiography 13(2):167–182

Snider RA, Serwer GA et al (1997) Echocardiography in pediatric heart disease. Mosby, St. Louis

Tacy TA, Silverman NH (2001) Systemic venous abnormalities: embryologic and echocardiographic considerations. Echocardiography 18(5):401–413

Villavicencio RE, Forbes TJ et al (2003) Pressure recovery in pediatric aortic valve stenosis. Pediatr Cardiol 24(5):457–462

Yoganathan AP, Valdes-Cruz LM et al (1987) Continuous-wave Doppler velocities and gradients across fixed tunnel obstructions: studies in vitro and in vivo. Circulation 76(3):657–666